An Efficient Labeled/Unlabeled Random Finite Set Algorithm for Multiobject Tracking

Thomas Kropfreiter, Florian Meyer, and Franz Hlawatsch

***Abstract*—We propose an efficient random finite set (RFS) based algorithm for multiobject tracking in which the object states are modeled by a combination of a labeled multi-Bernoulli (LMB) RFS and a Poisson RFS. The less computationally demanding Poisson part of the algorithm is used to track potential objects whose existence is unlikely. Only if a quantity characterizing the plausibility of object existence is above a threshold, a new labeled Bernoulli component is created and the object is tracked by the more accurate but more computationally demanding LMB part of the algorithm. Conversely, a labeled Bernoulli component is transferred back to the Poisson RFS if the corresponding existence probability falls below another threshold. Contrary to existing hybrid algorithms based on multi-Bernoulli and Poisson RFSs, the proposed method facilitates track continuity and implements complexity-reducing features. Simulation results demonstrate a large complexity reduction relative to other RFS-based algorithms with comparable performance.**

***Index Terms*—Filtering, multiobject tracking, multitarget tracking, object detection, point processes, random finite sets, sequential estimation.**

I. Introduction

Multiobject tracking aims to estimate the time-dependent states of an unknown, time-dependent number of objects from a sequence of measurements [1]–[5]. This task is complicated by a measurement-origin uncertainty, i.e., the fact that it is unknown which measurement was generated by which object. Most established multiobject tracking algorithms address measurement-origin uncertainty by solving a data association problem [1]. Here, we propose a multiobject tracking algorithm that uses random finite sets (RFSs) and the framework of finite set statistics (FISST) [2], [3] to model the object states and measurements.

A. State of the Art

Existing RFS-based multiobject tracking methods include the probability hypothesis density (PHD) filter [2], [6], the cardinalized PHD (CPHD) filter [2], [7], and multi-Bernoulli (MB) filters [2], [3], [8]. These filters do not require a data association step. They have a low or moderate computational complexity but can exhibit poor accuracy in more challenging scenarios. They do not maintain track continuity, in that they do not estimate entire trajectories of consecutive object states.

In many applications, track continuity is required. A widely used approach to achieving track continuity is to model the multiobject state by a labeled RFS [9]–[16]. Related tracking filters include the generalized labeled multi-Bernoulli (GLMB) filter [9], [10], [14], which is based on the GLMB RFS, and the labeled multi-Bernoulli (LMB) filter [11]–[13], which is based on the LMB RFS. Compared to the GLMB filter, the LMB filter incorporates certain approximations resulting in a much lower complexity. Recently, (G)LMB methods that are suitable for large-scale tracking scenarios [12]–[15] and that consider information from multiple consecutive measurements at each filtering step [16] have been proposed. On the other hand, the track-oriented marginal multi-Bernoulli/Poisson (TOMB/P) filter [17] is based on the union of two unlabeled RFSs, namely, a Poisson RFS and an MB RFS. The TOMB/P filter creates a new Bernoulli component for each measurement and prunes Bernoulli components with low existence probability. A modification of the TOMB/P filter [18] transfers Bernoulli components with low existence probability to the Poisson RFS instead of pruning them; this transfer is referred to as *recycling* in [18]. A "label-augmented" version of the TOMB/P filter that maintains track continuity was obtained in [19] by heuristically introducing labels in the formulation of the TOMB/P filter.

An alternative approach to multiobject tracking with track continuity is the paradigm of partially distinguishable populations [20]. This approach can lead to methods with a computational complexity that is linear in the number of tracks and the number of measurements.[1] Finally, track continuity can be achieved by modeling the multiobject state as an RFS of trajectories [21]–[24], where each trajectory is characterized by its initial time, its length, and the sequence of object states it contains. Algorithms based on this approach comprise the trajectory PHD and CPHD filters [23], the trajectory multi-Bernoulli mixture filter [21], and the trajectory Poisson multi-Bernoulli mixture filter [22]. These methods can have performance advantages over the methods proposed in [9]–[15], [17]–[20], but also a significantly increased computational complexity.

T. Kropfreiter and F. Hlawatsch are with the Institute of Telecommunications, TU Wien, 1040 Vienna, Austria (e-mail: {thomas.kropfreiter, franz.hlawatsch}@tuwien.ac.at). F. Meyer is with the Scripps Institution of Oceanography and the Department of Electrical and Computer Engineering, University of California San Diego, La Jolla, CA 92037, USA (e-mail: flmeyer@ucsd.edu). This work was supported by the Austrian Science Fund (FWF) under grant P 32055-N31, by the Czech Science Foundation (GAČR) under grant 17-19638S, and by the Office of Naval Research (ONR) under grant N00014-21-1-2267. Parts of this paper were previously presented at SDF 2018, Bonn, Germany, October 2018.

[1] Although relying on a different theoretical paradigm, the concept of distinguishable versus indistinguishable objects is partly similar to our concept of labeled versus unlabeled objects. However, whereas indistinguishable/unlabeled objects are considered in both approaches as an entity (modeled by a Poisson RFS in our method), in our approach also unlabeled objects are tracked within the Poisson part, i.e., the Poisson part is also updated by measurements. Furthermore, in [20] track continuity is achieved by using partially distinguishable populations, whereas in our method it is achieved by using a labeled RFS. Finally, the two methods employ different approximations to reduce computational complexity.

B. Contribution

Here, we propose a multiobject tracking algorithm with track continuity, termed LMB/P filter, that combines the strengths of the LMB filter and the PHD filter and is inspired by the label-augmented TOMB/P filter. We model the multiobject state as a combination of an LMB RFS (i.e., a labeled RFS) and a Poisson RFS (i.e., an unlabeled RFS). Whereas in the TOMB/P filter the Poisson RFS facilitates the creation of new Bernoulli components, the proposed LMB/P filter extends the use of the Poisson RFS to the tracking of "unlikely" objects. Only if a quantity characterizing the plausibility of object existence is above a threshold, the LMB/P filter creates a new labeled Bernoulli component, and the corresponding object is tracked within the more accurate but less efficient LMB part. Conversely, the LMB/P filter transfers labeled Bernoulli components to the Poisson RFS if the probability of object existence falls below another threshold. The fact that unlikely objects are tracked within the more efficient Poisson part results in a large reduction of computational complexity.

Our derivation of the proposed LMB/P filter is based on a new system model for labeled/unlabeled objects in which the multiobject state is modeled by a tuple of a labeled RFS and an unlabeled RFS. This system model is interesting in its own right as a basis for deriving further new labeled/unlabeled multiobject tracking filters.

The proposed LMB/P filter is rooted in the framework of Bayes-optimal multiobject tracking and employs several approximations to achieve computational feasibility and efficiency. Since an exact implementation of the Bayes-optimal multiobject tracking filter is computationally infeasible, certain approximations are employed by all practical multiobject tracking algorithms. For example, in the popular PHD filter, the posterior multiobject pdf is approximated by a Poisson pdf. While this is a rather strong approximation, it can be motivated and justified by the fact that the PHD filter has a very low computational complexity while still achieving good performance in multiobject tracking scenarios of low to moderate difficulty.

The proposed LMB/P filter employs a sequence of approximations that are considerably less severe and more sophisticated. Our goal is to combine the strengths of the PHD and LMB filters. In fact, the LMB/P filter can be interpreted as a combination of an LMB filter and a PHD filter that run in parallel but not independently of each other, even though the update relations of the PHD part are different from the update relations of the original PHD filter. The derivation of our filter is based on approximating the posterior multiobject pdf by a combined LMB–Poisson pdf. To further decrease the computational complexity, we introduce certain additional approximations and modifications. More specifically, we propose a clustering scheme based on a new criterion in order to reduce the complexity of data association, and we employ a flexible transfer between labeled and unlabeled objects in order to track "unlikely" objects with low complexity and "likely" objects with high accuracy. These approximations can be justified by the fact that they result in a low complexity and an excellent performance even in challenging multiobject tracking scenarios.

This paper differs from our conference publication [25] in that it proposes an improved label and measurement partitioning scheme, which results in a lower complexity; it presents a detailed derivation of the approximations used in the update step; it provides a detailed step-by-step statement of the proposed algorithm; and it presents an improved experimental performance evaluation. Furthermore, the proposed method differs from the TOMB/P filter with recycling [18] in that it uses a labeled RFS in order to facilitate track continuity, it incorporates a label and measurement partitioning scheme resulting in a complexity reduction, and it updates the Poisson RFS based on measurements that are unlikely to originate from a labeled object.

C. Paper Organization and Notation

The remainder of this paper is organized as follows. After a brief review of RFSs in Section II, Section III presents a system model for labeled/unlabeled objects. The prediction step and (exact) update step are presented in Sections IV and V, respectively. In Sections VI and VII, we describe the complexity-reducing approximations used in the update step of the LMB/P filter. Section VIII summarizes the LMB/P filter algorithm. Simulation results are presented in Section IX.

We will use the following notation. Vectors are denoted by small boldface letters (e.g., $\boldsymbol{x}$), unlabeled finite sets by capital letters (e.g., X), and labeled finite sets by capital letters with a tilde (e.g., $\tilde{X}$). Labeled states are denoted as $(\boldsymbol{x}, l)$, where $\boldsymbol{x}$ is a state vector and l is a label. Randomness is indicated by a sans serif font, such as in x or X. We write probability density functions (pdfs) as $f(\cdot)$ or $s(\cdot)$ and probability mass functions (pmfs) as $p(\cdot)$. The expectation operator is denoted by $\mathrm{E}\{\cdot\}$ and the probability by $\Pr\{\cdot\}$. Integrals are over the entire space of the integration variable unless noted otherwise. The superscript $^{\mathrm{T}}$ indicates transposition, and $\mathbf{I}_N$ denotes the $N \times N$ identity matrix.

II. Fundamentals of RFSs

A. Unlabeled RFSs

An (unlabeled) RFS $\mathsf{X} = \{\mathsf{x}^{(1)}, \ldots, \mathsf{x}^{(\mathsf{n})}\}$ is a random variable whose realizations X are finite sets $\{\boldsymbol{x}^{(1)}, \ldots, \boldsymbol{x}^{(n)}\}$ of vectors $\boldsymbol{x}^{(i)} \in \mathbb{R}^{n_x}$. Both the vectors $\mathsf{x}^{(i)}$ and their number $\mathsf{n} = |\mathsf{X}|$ (the cardinality of X) are random, and the elements $\mathsf{x}^{(i)}$ are unordered. We define $\rho(n) \triangleq \Pr\{|\mathsf{X}| = n\}$ as the pmf of the cardinality $\mathsf{n} = |\mathsf{X}|$. The *set integral* $\int g(X)\delta X$ of a real-valued set function $g(X)$ is defined as described in [2].

The statistics of an RFS X can be described by the *multiobject pdf* $f_{\mathsf{X}}(X)$, briefly denoted $f(X)$, or equivalently by the *probability generating functional* (pgfl) [2]

$$G_{\mathsf{X}}[h] \triangleq \int h^X f(X)\delta X.$$

Here, $h^X \triangleq \prod_{\boldsymbol{x}\in X} h(\boldsymbol{x})$, where $h\colon \mathbb{R}^{n_x} \to [0,\infty)$ is any nonnegative vector function. The pgfl of the union $\mathsf{X} = \bigcup_{j=1}^{J} \mathsf{X}^{(j)}$ of statistically independent RFSs $\mathsf{X}^{(j)}$, $j \in \mathcal{J} \triangleq \{1, \ldots, J\}$ is the product of the individual pgfls $G_{\mathsf{X}^{(j)}}[h]$, i.e,

$$G_{\mathsf{X}}[h] = \prod_{j\in\mathcal{J}} G_{\mathsf{X}^{(j)}}[h]. \tag{1}$$

The *PHD* or *intensity function* $\lambda_{\mathsf{X}}(\boldsymbol{x})\colon \mathbb{R}^{n_x}\to[0,\infty)$ of an RFS X, briefly denoted $\lambda(\boldsymbol{x})$, is a first-order moment of X with the property that for any region $\mathcal{S}\subseteq\mathbb{R}^{n_x}$, the integral $\int_{\mathcal{S}}\lambda(\boldsymbol{x})\mathrm{d}\boldsymbol{x}$ yields the expected number of objects whose states are located in that region, i.e., $\mathrm{E}\{|\mathsf{X}\cap S|\}=\int|X\cap S|\,f(X)\,\delta X$. The PHD can be obtained from the pgfl according to

$$\lambda(\boldsymbol{x}) = \frac{\delta}{\delta\boldsymbol{x}} G_{\mathsf{X}}[h]\bigg|_{h=1}, \tag{2}$$

where $\frac{\delta}{\delta\boldsymbol{x}}G_{\mathsf{X}}[h]$ denotes the functional derivative of $G_{\mathsf{X}}[h]$ [2].

For a *Poisson RFS*, the cardinality n is Poisson distributed with mean μ, i.e., $\rho(n)=e^{-\mu}\mu^n/n!$, $n\in\mathbb{N}_0$. For each cardinality $\mathsf{n}=|\mathsf{X}|$, the individual elements x are independent and identically distributed (iid) with some "spatial pdf" $f(\boldsymbol{x})$. The pgfl is [2]

$$G_{\mathsf{X}}[h] = P[h;\lambda] \triangleq e^{\lambda[h-1]}, \tag{3}$$

where $\lambda[h-1]=\int(h(\boldsymbol{x})-1)\,\lambda(\boldsymbol{x})\mathrm{d}\boldsymbol{x}$, and the PHD (intensity function) is $\lambda(\boldsymbol{x})=\mu f(\boldsymbol{x})$.

A *Bernoulli RFS* is parametrized by a probability of existence r and a spatial pdf $s(\boldsymbol{x})$. It is either empty with probability $1-r$ or it contains one element $\mathsf{x}\sim s(\boldsymbol{x})$ with probability r. The pgfl is [2]

$$G_{\mathsf{X}}[h] = B[h;r,s] \triangleq 1-r+r\,s[h], \tag{4}$$

with $s[h]=\int h(\boldsymbol{x})\,s(\boldsymbol{x})\mathrm{d}\boldsymbol{x}$. A linear combination of Bernoulli pgfls is again a Bernoulli pgfl: more specifically, for weights γ_i satisfying $\gamma_i\geq 0$ and $\sum_i\gamma_i=1$, we have

$$\sum_i \gamma_i B\big[h;r^{(i)},s^{(i)}\big] = B[h;r,s], \tag{5}$$

where

$$r=\sum_i\gamma_i r^{(i)}, \quad s(\boldsymbol{x})=\frac{1}{r}\sum_i\gamma_i r^{(i)}s^{(i)}(\boldsymbol{x}). \tag{6}$$

An *MB RFS* is the union of a fixed number J of statistically independent Bernoulli RFSs $\mathsf{X}^{(j)}$, $j\in\mathcal{J}$ parametrized by possibly different probabilities of existence $r^{(j)}$ and spatial pdfs $s^{(j)}(\boldsymbol{x})$. The pgfl is (cf. (1) and (4))

$$G_{\mathsf{X}}[h] = M_{\mathcal{J}}\big[h;r^{(\cdot)},s^{(\cdot)}\big] \triangleq \prod_{j\in\mathcal{J}} B\big[h;r^{(j)},s^{(j)}\big], \tag{7}$$

where $s^{(j)}[h]=\int h(\boldsymbol{x})\,s^{(j)}(\boldsymbol{x})\mathrm{d}\boldsymbol{x}$. Here, the superscript $^{(\cdot)}$ used in $M_{\mathcal{J}}\big[h;r^{(\cdot)},s^{(\cdot)}\big]$ indicates that $M_{\mathcal{J}}\big[h;r^{(\cdot)},s^{(\cdot)}\big]$ involves the set of existence probabilities $\{r^{(j)}\}_{j\in\mathcal{J}}$ and the set of spatial pdfs $\{s^{(j)}(\boldsymbol{x})\}_{j\in\mathcal{J}}$.

B. Labeled RFSs

In a labeled RFS $\tilde{\mathsf{X}}$, each element is a tuple of the form $(\mathsf{x},\mathsf{l})\in\mathbb{R}^{n_x}\times\mathbb{L}$, where the label space $\mathbb{L}$ is a countable set. Thus, a realization of $\tilde{\mathsf{X}}$ has the form $\tilde{X}=\big\{(\boldsymbol{x}^{(1)},l^{(1)}),\ldots,(\boldsymbol{x}^{(n)},l^{(n)})\big\}$. The set integral $\int g(\tilde{X})\,\delta\tilde{X}$ of a real-valued function $g(\tilde{X})$ can be defined as described in [3], [9]. Analogously to an unlabeled RFS, the statistics of a labeled RFS can be described by the multiobject pdf $f(\tilde{X})$ [3], [9], [10] or by the pgfl $G_{\tilde{\mathsf{X}}}[\tilde{h}]\triangleq\int\tilde{h}^{\tilde{X}}f(\tilde{X})\,\delta\tilde{X}$ [3, p. 449], where $\tilde{h}^{\tilde{X}}\triangleq\prod_{(\boldsymbol{x},l)\in\tilde{X}}\tilde{h}(\boldsymbol{x},l)$ with $\tilde{h}\colon\mathbb{R}^{n_x}\times\mathbb{L}\to[0,\infty)$.

An *LMB RFS* $\tilde{\mathsf{X}}$ is an MB RFS where for any realization $\tilde{X}$ each single-vector set $\{\boldsymbol{x}\}$ corresponding to a Bernoulli component $\mathsf{X}^{(j)}$ is augmented by a distinct label $l\in\mathbb{L}^*$. Here, adopting the labeling procedure of [3], the *same* label l is assigned to each state realization $\boldsymbol{x}$ of a given Bernoulli component $\mathsf{X}^{(j)}$, and $\mathbb{L}^*\subseteq\mathbb{L}$ denotes the finite set of assigned labels. To simplify the notation, we index the Bernoulli RFSs directly by their labels l, i.e., they are denoted $\mathsf{X}^{(l)}$, $l\in\mathbb{L}^*$ with corresponding existence probabilities $r^{(l)}$ and spatial distributions $s^{(l)}(\boldsymbol{x})$ [11]. The LMB RFS $\tilde{\mathsf{X}}$ is completely specified by the parameter set $\big\{\big(r^{(l)},s^{(l)}(\boldsymbol{x})\big)\big\}_{l\in\mathbb{L}^*}$. The pgfl is given by [3]

$$G_{\tilde{\mathsf{X}}}[\tilde{h}] = L_{\mathbb{L}^*}\big[\tilde{h},r^{(\cdot)},s^{(\cdot)}\big] \triangleq \prod_{l\in\mathbb{L}^*} B\big[\tilde{h};r^{(l)},s^{(l)}\big], \tag{8}$$

with $s^{(l)}[\tilde{h}]=\int\tilde{h}(\boldsymbol{x},l)\,s^{(l)}(\boldsymbol{x})\mathrm{d}\boldsymbol{x}$ (cf. (4)).

An *LMB mixture (LMBM) RFS* generalizes the LMB RFS in that its pgfl is a mixture of a finite number of LMB pgfls with identical label set $\mathbb{L}^*$, i.e.,

$$\begin{aligned} G_{\tilde{\mathsf{X}}}[\tilde{h}] &= \sum_i w_i\, L_{\mathbb{L}^*}\big[\tilde{h},r^{(\cdot,i)},s^{(\cdot,i)}\big] \\ &= \sum_i w_i \prod_{l\in\mathbb{L}^*} B\big[\tilde{h};r^{(l,i)},s^{(l,i)}\big]. \end{aligned}$$

Here, the weights satisfy $w_i\geq 0$ and $\sum_i w_i=1$, and $s^{(l,i)}[\tilde{h}]=\int\tilde{h}(\boldsymbol{x},l)\,s^{(l,i)}(\boldsymbol{x})\mathrm{d}\boldsymbol{x}$.

III. System Model

In this section, we present a new labeled/unlabeled RFS-based system model that provides statistical descriptions of the state evolution process and the measurement process. The proposed model is valid for all types of labeled/unlabeled multiobject state RFSs; the specific RFS type used for the multiobject state in our LMB/P filter will be described in Section IV. The multiobject state is composed of a labeled RFS part and an unlabeled RFS part. The labeled RFS part encodes the identities of the modeled objects and thus allows these objects to be distinguished. By contrast, the objects modeled by the unlabeled RFS part are indistinguishable.

More specifically, the multiobject state at time $k-1$ is constituted by the tuple $(\tilde{\mathsf{X}}_{k-1},\mathsf{X}_{k-1})$ of a labeled RFS $\tilde{\mathsf{X}}_{k-1}$ and an unlabeled RFS X_{k-1}. The elements of $\tilde{\mathsf{X}}_{k-1}$ are random tuples $(\mathsf{x}_{k-1},\mathsf{l})\in\mathbb{R}^{n_x}\times\mathbb{L}^*_{k-1}$, while the elements of X_{k-1} are random vectors $\mathsf{x}_{k-1}\in\mathbb{R}^{n_x}$. Here, x_{k-1} typically consists of the object's position and possibly further parameters, and $\mathbb{L}^*_{k-1}$ is the set of labels corresponding to $\tilde{\mathsf{X}}_{k-1}$, which is a subset of the label space $\mathbb{L}_{k-1}=\{1,\ldots,k-1\}\times\mathbb{N}$. Each label $l\in\mathbb{L}_{k-1}$ is a tuple of the form $l=(k',\nu)$, where $k'\in\{1,\ldots,k-1\}$ represents the object's time of birth and $\nu\in\mathbb{N}$ distinguishes objects born at the same time.

A. State-Evolution Model

The state-evolution model describes the statistics of the multiobject state at time k, $(\tilde{\mathsf{X}}_k,\mathsf{X}_k)$, for a given multiobject state at time $k-1$, $(\tilde{X}_{k-1},X_{k-1})$, as detailed in what follows. At time $k-1$, an object with labeled state $(\boldsymbol{x}_{k-1},l)\in\tilde{X}_{k-1}$ either survives with probability $p_{\mathrm{S}}(\boldsymbol{x}_{k-1},l)$

or dies with probability $1-p_{\mathrm{S}}(\boldsymbol{x}_{k-1},l)$. If it survives, its new state x_k (without the label l) is distributed according to the transition pdf $f(\boldsymbol{x}_k|\boldsymbol{x}_{k-1},l)$, and the label is preserved by the state transition. This means that the labels of surviving objects do not change, and thus we denote them as l rather than l_k. The states of different objects evolve independently, i.e.,[2] (x_k,l) is conditionally independent, given $(\boldsymbol{x}_{k-1},l)$, of all (x'_k,l') with $l'\neq l$ and also of all states $\mathsf{x}''_k\in\mathsf{X}_k$. Due to these assumptions, the multiobject state of the labeled objects at time k, given $(\tilde{X}_{k-1},X_{k-1})$, is described by an LMB RFS (see Section II-B)

$$\tilde{\mathsf{X}}_k=\bigcup_{l\in\mathbb{L}^*_{k-1}}\tilde{\mathsf{S}}_k(\boldsymbol{x}_{k-1},l),$$

where $\tilde{\mathsf{S}}_k(\boldsymbol{x}_{k-1},l)$ is a labeled Bernoulli RFS with existence probability $r_k^{(l)}=p_{\mathrm{S}}(\boldsymbol{x}_{k-1},l)$ and spatial pdf $s_k^{(l)}(\boldsymbol{x}_k)=f(\boldsymbol{x}_k|\boldsymbol{x}_{k-1},l)$. Thus, $\tilde{\mathsf{X}}_k$ is characterized by the Bernoulli parameter set $\big\{\big(p_{\mathrm{S}}(\boldsymbol{x}_{k-1},l),f(\boldsymbol{x}_k|\boldsymbol{x}_{k-1},l)\big)\big\}_{l\in\mathbb{L}^*_{k-1}}$.

Furthermore, at time $k-1$, an object with unlabeled state $\boldsymbol{x}_{k-1}\in X_{k-1}$ either survives with probability[3] $p_{\mathrm{S}}(\boldsymbol{x}_{k-1})$ or dies with probability $1-p_{\mathrm{S}}(\boldsymbol{x}_{k-1})$. If it survives, its new state x_k is distributed according to the transition pdf $f(\boldsymbol{x}_k|\boldsymbol{x}_{k-1})$. The states of different unlabeled objects evolve independently, i.e., x_k is conditionally independent, given $\boldsymbol{x}_{k-1}$, of all the other x'_k and also of the states $(\mathsf{x}''_k,\mathsf{l})\in\tilde{\mathsf{X}}_k$. Accordingly, the multiobject state of the survived unlabeled objects at time k, given $(\tilde{X}_{k-1},X_{k-1})$, is modeled as an MB RFS (see Section II-A) $\mathsf{X}_k^{\mathrm{S}}=\bigcup_{\boldsymbol{x}_{k-1}\in X_{k-1}}\mathsf{S}_k(\boldsymbol{x}_{k-1})$, where $\mathsf{S}_k(\boldsymbol{x}_{k-1})$ is a Bernoulli RFS with parameters $r_k=p_{\mathrm{S}}(\boldsymbol{x}_{k-1})$ and $s_k(\boldsymbol{x}_k)=f(\boldsymbol{x}_k|\boldsymbol{x}_{k-1})$. Thus, $\mathsf{X}_k^{\mathrm{S}}$ is characterized by the Bernoulli parameter set $\big\{\big(p_{\mathrm{S}}(\boldsymbol{x}_{k-1}),f(\boldsymbol{x}_k|\boldsymbol{x}_{k-1})\big)\big\}_{\boldsymbol{x}_{k-1}\in X_{k-1}}$.

Object birth is modeled by an (unlabeled) Poisson RFS $\mathsf{X}_k^{\mathrm{B}}$ with mean parameter μ_{B} and spatial pdf $f_{\mathrm{B}}(\boldsymbol{x}_k)$ and, hence, PHD $\lambda_k^{\mathrm{B}}(\boldsymbol{x}_k)=\mu_{\mathrm{B}}f_{\mathrm{B}}(\boldsymbol{x}_k)$.[4] Thus, the entirety of unlabeled objects at time k, given $(\tilde{X}_{k-1},X_{k-1})$, is described by the RFS

$$\mathsf{X}_k=\mathsf{X}_k^{\mathrm{S}}\cup\mathsf{X}_k^{\mathrm{B}}=\left(\bigcup_{\boldsymbol{x}_{k-1}\in X_{k-1}}\mathsf{S}_k\big(\boldsymbol{x}_{k-1}\big)\right)\cup\mathsf{X}_k^{\mathrm{B}}.$$

We assume that all newborn unlabeled object states $\mathsf{x}_k\in\mathsf{X}_k^{\mathrm{B}}$ are independent of all $\mathsf{x}'_k\in\mathsf{X}_k$, all $(\mathsf{x}''_k,l)\in\tilde{\mathsf{X}}_k$, and all measurements (see below) $\mathsf{z}_k\in\mathsf{Z}_k$. Due to our above independence assumptions, the RFSs $\mathsf{X}_k^{\mathrm{S}}$ and $\mathsf{X}_k^{\mathrm{B}}$ are conditionally independent given $\big(\tilde{X}_{k-1},X_{k-1}\big)$.

[2]We note that (x_k,l) is short for $(\mathsf{x}_k,\mathsf{l}=l)$, which denotes the state of an object with a specific (thus, deterministic) label l, whereas $(\mathsf{x}_k,\mathsf{l})$ denotes the state of an object with an arbitrary (thus, random) label l.

[3]With an abuse of notation, $p_{\mathrm{S}}(\cdot)$ is used to denote both the survival probability of labeled objects (with argument $(\boldsymbol{x}_{k-1},l)$) and of unlabeled objects (with argument $\boldsymbol{x}_{k-1}$). A similar remark applies to the detection probability $p_{\mathrm{D}}(\cdot)$ considered in Section III-B.

[4]In our system model, newborn objects may not be labeled objects. As we will explain in Section V-A, there do exist "new" labeled objects, which are previously unlabeled objects that are augmented by a new distinct label and thereby are transferred from the unlabeled RFS to the labeled RFS. Thus, this creation of new labeled objects is not modeled by a birth process as in the LMB filter [11]; it is considered as a part of the tracking algorithm, rather than of the system model.

B. Measurement Model

At time k, a sensor produces M_k measurements $\mathsf{z}_k^{(1)},\ldots,\mathsf{z}_k^{(\mathsf{M}_k)}$, which are modeled as an (unlabeled) RFS $\mathsf{Z}_k\triangleq\big\{\mathsf{z}_k^{(1)},\ldots,\mathsf{z}_k^{(\mathsf{M}_k)}\big\}$.[5] The measurements may originate from a labeled object, an unlabeled object, or clutter.

A labeled object with state $(\boldsymbol{x}_k,l)\in\tilde{X}_k$ is detected (i.e., it generates a measurement) with probability $p_{\mathrm{D}}(\boldsymbol{x}_k,l)$ or is missed (i.e., it does not generate a measurement) with probability $1-p_{\mathrm{D}}(\boldsymbol{x}_k,l)$. In the first case, the object generates exactly one measurement z_k, which is distributed according to the likelihood function $f(\boldsymbol{z}_k|\boldsymbol{x}_k,l)$. We assume that z_k is conditionally independent, given $(\boldsymbol{x}_k,l)$, of all the other z'_k, all the other $(\mathsf{x}'_k,\mathsf{l}')\in\tilde{\mathsf{X}}_k$, and all the $\mathsf{x}''_k\in\mathsf{X}_k$. Accordingly, the measurements originating from labeled objects, given $(\tilde{X}_k,X_k)$, are modeled by an MB RFS $\mathsf{Z}_k^{\mathrm{L}}=\bigcup_{l\in\mathbb{L}^*_{k-1}}\Theta_k^{\mathrm{L}}(\boldsymbol{x}_k,l)$, where $\Theta_k^{\mathrm{L}}(\boldsymbol{x}_k,l)$ is a Bernoulli RFS with parameters $r_k^{(l)}=p_{\mathrm{D}}(\boldsymbol{x}_k,l)$ and $s^{(l)}(\boldsymbol{x}_k)=f(\boldsymbol{z}_k|\boldsymbol{x}_k,l)$. Thus, $\mathsf{Z}_k^{\mathrm{L}}$ is characterized by the Bernoulli parameter set $\big\{\big(p_{\mathrm{D}}(\boldsymbol{x}_k,l),f(\boldsymbol{z}_k|\boldsymbol{x}_k,l)\big)\big\}_{l\in\mathbb{L}^*_{k-1}}$.

An unlabeled object with state $\boldsymbol{x}_k\in X_k$ is detected with probability $p_{\mathrm{D}}(\boldsymbol{x}_k)$ or is missed with probability $1-p_{\mathrm{D}}(\boldsymbol{x}_k)$. In the first case, it generates exactly one measurement z_k, which is distributed according to the likelihood function $f(\boldsymbol{z}_k|\boldsymbol{x}_k)$. We assume that z_k is conditionally independent, given $\boldsymbol{x}_k$, of all the other z'_k, all the other $\mathsf{x}'_k\in\mathsf{X}_k$, and all the $(\mathsf{x}''_k,\mathsf{l})\in\tilde{\mathsf{X}}_k$. Hence, the measurements originating from unlabeled objects, given $(\tilde{X}_k,X_k)$, are modeled by an MB RFS $\mathsf{Z}_k^{\mathrm{U}}=\bigcup_{\boldsymbol{x}_k\in X_k}\Theta_k^{\mathrm{U}}(\boldsymbol{x}_k)$, where $\Theta_k^{\mathrm{U}}(\boldsymbol{x}_k)$ is a Bernoulli RFS with parameters $r_k=p_{\mathrm{D}}(\boldsymbol{x}_k)$ and $s(\boldsymbol{x}_k)=f(\boldsymbol{z}_k|\boldsymbol{x}_k)$. Thus, $\mathsf{Z}_k^{\mathrm{U}}$ is characterized by the Bernoulli parameter set $\big\{\big(p_{\mathrm{D}}(\boldsymbol{x}_k),f(\boldsymbol{z}_k|\boldsymbol{x}_k)\big)\big\}_{\boldsymbol{x}_k\in X_k}$.

Finally, the clutter-originated measurements are modeled by a Poisson RFS $\mathsf{Z}_k^{\mathrm{C}}$ with mean parameter μ_{C} and spatial pdf $f_{\mathrm{C}}(\boldsymbol{z}_k)$ and, hence, PHD $\lambda_k^{\mathrm{C}}(\boldsymbol{z}_k)=\mu_{\mathrm{C}}f_{\mathrm{C}}(\boldsymbol{z}_k)$. It thus follows that the overall measurement RFS at time k, given the multiobject state $(\tilde{X}_k,X_k)$, is

$$\begin{aligned}\mathsf{Z}_k&=\mathsf{Z}_k^{\mathrm{L}}\cup\mathsf{Z}_k^{\mathrm{U}}\cup\mathsf{Z}_k^{\mathrm{C}}\\&=\left(\bigcup_{l\in\mathbb{L}^*_{k-1}}\Theta_k^{\mathrm{L}}(\boldsymbol{x}_k,l)\right)\cup\left(\bigcup_{\boldsymbol{x}_k\in X_k}\Theta_k^{\mathrm{U}}(\boldsymbol{x}_k)\right)\cup\mathsf{Z}_k^{\mathrm{C}}.\end{aligned}$$

We assume that all clutter-originated measurements $\mathsf{z}_k\in\mathsf{Z}_k^{\mathrm{C}}$ are independent of all $\mathsf{z}'_k\in\mathsf{Z}_k^{\mathrm{U}}$ and $\mathsf{z}''_k\in\mathsf{Z}_k^{\mathrm{L}}$ and all $(\mathsf{x}_k,\mathsf{l})\in\tilde{\mathsf{X}}_k$ and $\mathsf{x}'_k\in\mathsf{X}_k$. Due to our above independence assumptions, the RFSs $\mathsf{Z}_k^{\mathrm{L}}$, $\mathsf{Z}_k^{\mathrm{U}}$, and $\mathsf{Z}_k^{\mathrm{C}}$ are conditionally independent given $(\tilde{X}_k,X_k)$. We note that equivalent independence assumptions, although possibly formulated in a different manner, underlie many established RFS-based [2], [3] and other [1], [4] tracking algorithms.

IV. Prediction Step

Adopting a Bayesian sequential inference framework, the fundamental quantity to be calculated recursively

[5]The measurement model describes the statistical dependence of the random (unobserved) measurements on the multiobject state. Accordingly, at this point, the measurements are considered random and thus denoted as $\mathsf{Z}_k=\big\{\mathsf{z}_k^{(1)},\ldots,\mathsf{z}_k^{(\mathsf{M}_k)}\big\}$. However, in the context of our tracking algorithm (see Sections V–VIII), the measurements will be considered as deterministic (observed) and will thus be denoted as $Z_k=\big\{\boldsymbol{z}_k^{(1)},\ldots,\boldsymbol{z}_k^{(M_k)}\big\}$.

is the joint posterior multiobject pdf of $\tilde{\mathsf{X}}_k$ and X_k, $f(\tilde{X}_k, X_k|Z_{1:k})$ with $Z_{1:k} \triangleq (Z_1, \ldots, Z_k)$, or equivalently the joint posterior pgfl $G_{\tilde{\mathsf{X}}_k,\mathsf{X}_k}[\tilde{h}, h|Z_{1:k}] \triangleq \int\int \tilde{h}^{\tilde{X}_k} h^{X_k} f(\tilde{X}_k, X_k|Z_{1:k})\, \delta\tilde{X}_k\, \delta X_k$. We make the simplifying approximation that, at the previous time $k-1$, $\tilde{\mathsf{X}}_{k-1}$ and X_{k-1} are conditionally independent given $Z_{1:k-1}$, so that

$$G_{\tilde{\mathsf{X}}_{k-1},\mathsf{X}_{k-1}}[\tilde{h}, h|Z_{1:k-1}] = G_{\tilde{\mathsf{X}}_{k-1}}[\tilde{h}]\, G_{\mathsf{X}_{k-1}}[h]. \tag{9}$$

(Note that in all pgfl factors and approximating pgfls, we suppress the conditions $Z_{1:k-1}$ and $Z_{1:k}$ for notational simplicity.) The above factorization will be preserved automatically over time. That is, using the proposed algorithm—in particular, the approximations in the update step described in Sections VI and VII—, the joint posterior pgfl will factor into a labeled part and an unlabeled part also at time k and at all future times.

The pgfl factors $G_{\tilde{\mathsf{X}}_{k-1}}[\tilde{h}]$ and $G_{\mathsf{X}_{k-1}}[h]$ in (9) are given as follows. We model $\tilde{\mathsf{X}}_{k-1}$ as an LMB RFS consisting of $|\mathbb{L}^*_{k-1}|$ labeled Bernoulli RFSs with existence probabilities $r^{(l)}_{k-1}$ and spatial pdfs $s^{(l)}_{k-1}(\boldsymbol{x}_{k-1})$, $l \in \mathbb{L}^*_{k-1}$. Here, $\mathbb{L}^*_{k-1} \subseteq \mathbb{L}_{k-1}$ is the set of labels underlying $\tilde{\mathsf{X}}_{k-1}$. Thus, according to (8),

$$G_{\tilde{\mathsf{X}}_{k-1}}[\tilde{h}] = \prod_{l\in\mathbb{L}^*_{k-1}} B\big[\tilde{h}; r^{(l)}_{k-1}, s^{(l)}_{k-1}\big], \tag{10}$$

where $s^{(l)}_{k-1}[\tilde{h}] = \int \tilde{h}(\boldsymbol{x}_{k-1}, l)\, s^{(l)}_{k-1}(\boldsymbol{x}_{k-1})\, \mathrm{d}\boldsymbol{x}_{k-1}$. Furthermore, we model X_{k-1} as a Poisson RFS with PHD $\lambda_{k-1}(\boldsymbol{x}_{k-1})$. Thus, according to (3),

$$G_{\mathsf{X}_{k-1}}[h] = P[h; \lambda_{k-1}]. \tag{11}$$

Taken together, Eqs. (9)–(11) express the fact that all the object states—both the labeled states, $(\mathbf{x}_{k-1}, \mathsf{l}) \in \tilde{\mathsf{X}}_{k-1}$, and the unlabeled states, $\mathbf{x}_{k-1} \in \mathsf{X}_{k-1}$—are conditionally independent given $Z_{1:k-1}$. A similar approximation, though formulated in a different manner, is used by many established RFS-based [2], [3] and other [1], [4] tracking algorithms.

The joint pgfl $G_{\tilde{\mathsf{X}}_{k-1},\mathsf{X}_{k-1}}[\tilde{h}, h|Z_{1:k-1}]$ in (9) represents the joint RFS $(\tilde{\mathsf{X}}_{k-1}, \mathsf{X}_{k-1})$. Since the elements of the labeled RFS $\tilde{\mathsf{X}}_{k-1}$ are defined on the space $\mathbb{R}^{n_x} \times \mathbb{L}^*_{k-1}$ and the elements of the unlabeled RFS X_{k-1} on the space $\mathbb{R}^{n_x}$, the elements of $(\tilde{\mathsf{X}}_{k-1}, \mathsf{X}_{k-1})$ are defined on the space $\mathbb{R}^{n_x} \times \mathbb{L}^*_{k-1} \times \mathbb{R}^{n_x}$. Accordingly, in (9), the LMB pgfl $G_{\tilde{\mathsf{X}}_{k-1}}[\tilde{h}]$ (cf. (10)) describes labeled object states that are defined on the space $\mathbb{R}^{n_x} \times \mathbb{L}^*_{k-1}$, and the Poisson pgfl $G_{\mathsf{X}_{k-1}}[h]$ (cf. (11)) describes unlabeled object states that are defined on the space $\mathbb{R}^{n_x}$.

As previously stated in Section III, the labeled state RFS, i.e, the LMB RFS $\tilde{\mathsf{X}}_{k-1}$, allows the corresponding objects to be distinguished, whereas the objects modeled by the unlabeled state RFS, i.e., the Poisson RFS X_{k-1}, are indistinguishable. On the other hand, the Poisson RFS is parametrized by a single function, i.e., its PHD, and it enables a much more efficient representation and processing of a large number of potentially existing objects. Therefore, we will model objects that are likely to exist by the computationally more demanding LMB part and objects that are unlikely to exist by the computationally less demanding Poisson part. The LMB part guarantees track continuity and thereby allows the consistent tracking of distinguishable objects over consecutive time steps.

The proposed LMB/P filter propagates the posterior pgfl $G_{\tilde{\mathsf{X}}_k,\mathsf{X}_k}[\tilde{h}, h|Z_{1:k}]$ from one time step to the next. This consists of a prediction step and an update step. In the prediction step, the previous posterior pgfl $G_{\tilde{\mathsf{X}}_{k-1},\mathsf{X}_{k-1}}[\tilde{h}, h|Z_{1:k-1}]$ given by (9)–(11) is converted into a predicted posterior pgfl $G_{\tilde{\mathsf{X}}_k,\mathsf{X}_k}[\tilde{h}, h|Z_{1:k-1}] \triangleq \int \tilde{h}^{\tilde{X}_k} h^{X_k} f(\tilde{X}_k, X_k|Z_{1:k-1})\, \delta\tilde{X}_k\, \delta X_k$, where $f(\tilde{X}_k, X_k|Z_{1:k-1})$ is the predicted posterior multiobject pdf. This conversion involves the state-transition parameters $p_{\mathrm{S}}(\boldsymbol{x}_{k-1}, l)$, $f(\boldsymbol{x}_k|\boldsymbol{x}_{k-1}, l)$, $p_{\mathrm{S}}(\boldsymbol{x}_{k-1})$, $f(\boldsymbol{x}_k|\boldsymbol{x}_{k-1})$, and $\lambda^{\mathrm{B}}_k(\boldsymbol{x}_k) = \mu_{\mathrm{B}}\, f_{\mathrm{B}}(\boldsymbol{x}_k)$ introduced in Section III-A.

The derivation of the prediction step is analogous to that in [17] but extends it from an unlabeled to a partly labeled multiobject state. Following [17], one obtains that the predicted posterior pgfl factors analogously to (9), i.e.,

$$G_{\tilde{\mathsf{X}}_k,\mathsf{X}_k}[\tilde{h}, h|Z_{1:k-1}] = G^{\mathrm{P}}_{\tilde{\mathsf{X}}_k}[\tilde{h}]\, G^{\mathrm{P}}_{\mathsf{X}_k}[h]. \tag{12}$$

Here, the factor $G^{\mathrm{P}}_{\tilde{\mathsf{X}}_k}[\tilde{h}]$ is of LMB form, i.e.,

$$G^{\mathrm{P}}_{\tilde{\mathsf{X}}_k}[\tilde{h}] = \prod_{l\in\mathbb{L}^*_{k-1}} B\big[\tilde{h}; r^{(l)}_{k|k-1}, s^{(l)}_{k|k-1}\big],$$

where

$$r^{(l)}_{k|k-1} = r^{(l)}_{k-1} \int p_{\mathrm{S}}(\boldsymbol{x}_{k-1}, l)\, s^{(l)}_{k-1}(\boldsymbol{x}_{k-1})\, \mathrm{d}\boldsymbol{x}_{k-1}, \tag{13}$$

$$s^{(l)}_{k|k-1}(\boldsymbol{x}_k) = \frac{\int f(\boldsymbol{x}_k|\boldsymbol{x}_{k-1}, l)\, p_{\mathrm{S}}(\boldsymbol{x}_{k-1}, l)\, s^{(l)}_{k-1}(\boldsymbol{x}_{k-1})\, \mathrm{d}\boldsymbol{x}_{k-1}}{\int p_{\mathrm{S}}(\boldsymbol{x}'_{k-1}, l)\, s^{(l)}_{k-1}(\boldsymbol{x}'_{k-1})\, \mathrm{d}\boldsymbol{x}'_{k-1}}, \tag{14}$$

for $l \in \mathbb{L}^*_{k-1}$. We recall that $r^{(l)}_{k-1}$ and $s^{(l)}_{k-1}(\boldsymbol{x}_{k-1})$ are the parameters of $G_{\tilde{\mathsf{X}}_{k-1}}[\tilde{h}]$ in (10). Relations (13) and (14) equal the prediction relations of the LMB filter [11].

The other factor in (12), $G^{\mathrm{P}}_{\mathsf{X}_k}[h]$, is not a Poisson pgfl anymore but a weighted Poisson pgfl [17]. Still following [17], we approximate it by the pgfl of the Poisson RFS whose PHD equals the PHD corresponding to $G^{\mathrm{P}}_{\mathsf{X}_k}[h]$. This yields

$$G^{\mathrm{P}}_{\mathsf{X}_k}[h] \approx P[h; \lambda_{k|k-1}], \tag{15}$$

with

$$\lambda_{k|k-1}(\boldsymbol{x}_k) = \lambda^{\mathrm{B}}_k(\boldsymbol{x}_k) + \int f(\boldsymbol{x}_k|\boldsymbol{x}_{k-1})\, p_{\mathrm{S}}(\boldsymbol{x}_{k-1})\, \lambda_{k-1}(\boldsymbol{x}_{k-1})\, \mathrm{d}\boldsymbol{x}_{k-1}. \tag{16}$$

Here, we recall that $\lambda_{k-1}(\boldsymbol{x}_{k-1})$ is the PHD corresponding to $G_{\mathsf{X}_{k-1}}[h]$ in (11) and $\lambda^{\mathrm{B}}_k(\boldsymbol{x}_k)$ is the birth PHD modeling the birth of objects as explained in Section III-A. We note that the above Poisson pgfl approximation is also used in the prediction step of the PHD filter [6], and in fact relation (16) equals the prediction relation of the PHD filter [6]. We furthermore note that the approximation can be interpreted as the minimization of a Kullback-Leibler divergence [26].

We conclude that when the approximation (15) is used, the prediction step preserves the LMB–Poisson form of the previous posterior pgfl $G_{\tilde{\mathsf{X}}_{k-1},\mathsf{X}_{k-1}}[\tilde{h}, h|Z_{1:k-1}]$.

V. Exact Update Step

In the update step, the predicted posterior pgfl $G_{\tilde{\mathsf{X}}_k,\mathsf{X}_k}[\tilde{h},h|Z_{1:k-1}]$ is converted into the new posterior pgfl at time k, $G_{\tilde{\mathsf{X}}_k,\mathsf{X}_k}[\tilde{h},h|Z_{1:k}]$. This conversion involves the current measurement set Z_k as well as the measurement parameters $p_{\mathrm{D}}(\boldsymbol{x}_k,l)$, $f(\boldsymbol{z}_k|\boldsymbol{x}_k,l)$, $p_{\mathrm{D}}(\boldsymbol{x}_k)$, $f(\boldsymbol{z}_k|\boldsymbol{x}_k)$, and $\lambda_k^{\mathrm{C}}(\boldsymbol{z}_k)=\mu_{\mathrm{C}}\,f_{\mathrm{C}}(\boldsymbol{z}_k)$ introduced in Section III-B. The derivation of the update step is again analogous to that in [17]. It turns out that $G_{\tilde{\mathsf{X}}_k,\mathsf{X}_k}[\tilde{h},h|Z_{1:k}]$ factors according to

$$G_{\tilde{\mathsf{X}}_k,\mathsf{X}_k}[\tilde{h},h|Z_{1:k}] = G'_{\tilde{\mathsf{X}}_k,\mathsf{X}_k}[\tilde{h},h]\,\bar{G}_{\mathsf{X}_k}[h], \tag{17}$$

where the factor $G'_{\tilde{\mathsf{X}}_k,\mathsf{X}_k}[\tilde{h},h]$ represents *detected objects* and the factor $\bar{G}_{\mathsf{X}_k}[h]$ *undetected objects*. Detected objects are labeled or unlabeled objects—either likely to exist or not—that generated a measurement in the current or a previous update step, while undetected objects are unlabeled objects that are unlikely to exist and did not generate a measurement in the current update step. Expressions of $G'_{\tilde{\mathsf{X}}_k,\mathsf{X}_k}[\tilde{h},h]$ and $\bar{G}_{\mathsf{X}_k}[h]$ will be provided in the next two subsections.

The "exact" update step discussed in this section has a high complexity. We emphasize that the update step of the proposed LMB/P filter is different in that it involves several complexity-reducing modifications and approximations, to be described in Sections VI and VII.

A. Expression of the pgfl of Detected Objects

Next, we will provide an expression of the pgfl of detected objects, $G'_{\tilde{\mathsf{X}}_k,\mathsf{X}_k}[\tilde{h},h]$. Let $\mathcal{M}_k \triangleq \{1,\ldots,M_k\}$ denote the set of measurement indices (cf. Section III-B). We introduce the random *association vector* $\mathsf{a}_k \in (\{0\}\cup\mathcal{M}_k)^{|\mathbb{L}^*_{k-1}|}$, whose entries $\mathsf{a}_k^{(l)}$, $l\in\mathbb{L}^*_{k-1}$ are given as $\mathsf{a}_k^{(l)} \triangleq m \in \mathcal{M}_k$ if the labeled object with state (x_k,l) generates measurement $\boldsymbol{z}_k^{(m)}$ and $\mathsf{a}_k^{(l)} \triangleq 0$ if it does not generate a measurement. Note that in the first case, the labeled object with state (x_k,l) is detected, and in the second case, it is missed. We call each possible value $\boldsymbol{a}_k$ of the association vector a_k an *association hypothesis*, and we call $\boldsymbol{a}_k$ *admissible* if all the nonzero entries $a_k^{(l)}$ are different, which implies that at most one measurement is assigned to a labeled object and no measurement is assigned to more than one labeled object. The *association alphabet* $\mathcal{A}_k$ is defined as the set of all admissible $\boldsymbol{a}_k$.

Using a_k, a derivation analogous to [17] shows that $G'_{\tilde{\mathsf{X}}_k,\mathsf{X}_k}[\tilde{h},h]$ is a mixture of pgfls, where each pgfl is the product of an LMB pgfl $L_{\mathbb{L}^*_{k-1}}\big[\tilde{h};r_k^{(\cdot,a_k^{(\cdot)})},s_k^{(\cdot,a_k^{(\cdot)})}\big]$ (see (8)) and an MB pgfl $M_{\mathcal{M}_{\boldsymbol{a}_k}}\big[h;\bar{r}_k^{(\cdot)},\bar{s}_k^{(\cdot)}\big]$ (see (7)), i.e.,

$$\begin{aligned} G'_{\tilde{\mathsf{X}}_k,\mathsf{X}_k}[\tilde{h},h] &= \sum_{\boldsymbol{a}_k\in\mathcal{A}_k} w_{\boldsymbol{a}_k}\, L_{\mathbb{L}^*_{k-1}}\big[\tilde{h};r_k^{(\cdot,a_k^{(\cdot)})},s_k^{(\cdot,a_k^{(\cdot)})}\big] \\ &\qquad \times M_{\mathcal{M}_{\boldsymbol{a}_k}}\big[h;\bar{r}_k^{(\cdot)},\bar{s}_k^{(\cdot)}\big] \qquad (18)\\ &= \sum_{\boldsymbol{a}_k\in\mathcal{A}_k} w_{\boldsymbol{a}_k}\Bigg(\prod_{l\in\mathbb{L}^*_{k-1}} B\big[\tilde{h};r_k^{(l,a_k^{(l)})},s_k^{(l,a_k^{(l)})}\big]\Bigg) \\ &\qquad \times \prod_{m\in\mathcal{M}_{\boldsymbol{a}_k}} B\big[h;\bar{r}_k^{(m)},\bar{s}_k^{(m)}\big]. \qquad (19)\end{aligned}$$

Here, $\mathcal{M}_{\boldsymbol{a}_k}\subseteq\mathcal{M}_k$ is the index set of all measurements that are not associated with any labeled object via $\boldsymbol{a}_k\in\mathcal{A}_k$; note in particular that $\mathcal{M}_{\boldsymbol{a}_k}=\emptyset$ indicates that all measurements are associated with labeled objects. Expressions of $r_k^{(l,a_k^{(l)})}$, $s_k^{(l,a_k^{(l)})}(\boldsymbol{x}_k)$ and $\bar{r}_k^{(m)}$, $\bar{s}_k^{(m)}(\boldsymbol{x}_k)$ will be presented shortly. Furthermore, the weights $w_{\boldsymbol{a}_k}$ in (18) and (19) are given up to a normalization constant by

$$w_{\boldsymbol{a}_k} \propto \Bigg(\prod_{l\in\mathbb{L}^*_{k-1}} \beta_k^{(l,a_k^{(l)})}\Bigg)\prod_{m\in\mathcal{M}_{\boldsymbol{a}_k}}\beta_k^{(m)}, \tag{20}$$

where $\beta_k^{(l,a_k^{(l)})}$ and $\beta_k^{(m)}$ are referred to as *association weights* [17]. Note that in (19), each mixture component corresponds to one of the admissible association hypotheses $\boldsymbol{a}_k\in\mathcal{A}_k$. The LMB pgfl $L_{\mathbb{L}^*_{k-1}}\big[\tilde{h};r_k^{(\cdot,a_k^{(\cdot)})},s_k^{(\cdot,a_k^{(\cdot)})}\big]$ represents objects that are likely to exist and are either detected or undetected in the current update step, and the MB pgfl $M_{\mathcal{M}_{\boldsymbol{a}_k}}\big[h;\bar{r}_k^{(\cdot)},\bar{s}_k^{(\cdot)}\big]$ represents objects that are unlikely to exist but, nevertheless, are detected in the current update step.

Next, we present expressions of $\beta_k^{(l,a_k^{(l)})}$, $r_k^{(l,a_k^{(l)})}$, and $s_k^{(l,a_k^{(l)})}(\boldsymbol{x}_k)$ for $l\in\mathbb{L}^*_{k-1}$ [17]. For $a_k^{(l)}=m\in\mathcal{M}_k$, we have

$$\beta_k^{(l,m)} = r_{k|k-1}^{(l)}\,b_k^{(l,m)}, \tag{21}$$

$$r_k^{(l,m)} = 1, \tag{22}$$

$$s_k^{(l,m)}(\boldsymbol{x}_k) = \frac{p_{\mathrm{D}}(\boldsymbol{x}_k,l)\,f\big(\boldsymbol{z}_k^{(m)}\big|\boldsymbol{x}_k,l\big)\,s_{k|k-1}^{(l)}(\boldsymbol{x}_k)}{b_k^{(l,m)}}, \tag{23}$$

with $b_k^{(l,m)} \triangleq \int p_{\mathrm{D}}(\boldsymbol{x}_k,l)\,f\big(\boldsymbol{z}_k^{(m)}\big|\boldsymbol{x}_k,l\big)\,s_{k|k-1}^{(l)}(\boldsymbol{x}_k)\,\mathrm{d}\boldsymbol{x}_k$. Here, $r_{k|k-1}^{(l)}$ and $s_{k|k-1}^{(l)}(\boldsymbol{x}_k)$ were calculated in the prediction step, see (13) and (14). Note that (22) indicates that the object with label l exists; its state $(\mathbf{x}_k,l)$ is distributed according to $s_k^{(l,m)}(\boldsymbol{x}_k)$ in (23). The plausibility of this event (i.e., that the object with state $(\mathbf{x}_k,l)$ exists and generates measurement $\boldsymbol{z}_k^{(m)}$) is quantified by $\beta_k^{(l,m)}$ in (21). On the other hand, for $a_k^{(l)}=0$, we have

$$\beta_k^{(l,0)} = 1 - r_{k|k-1}^{(l)} + r_{k|k-1}^{(l)}c_k^{(l)}, \tag{24}$$

$$r_k^{(l,0)} = \frac{r_{k|k-1}^{(l)}c_k^{(l)}}{\beta_k^{(l,0)}}, \tag{25}$$

$$s_k^{(l,0)}(\boldsymbol{x}_k) = \frac{\big(1-p_{\mathrm{D}}(\boldsymbol{x}_k,l)\big)\,s_{k|k-1}^{(l)}(\boldsymbol{x}_k)}{c_k^{(l)}}, \tag{26}$$

with $c_k^{(l)} \triangleq \int\big(1-p_{\mathrm{D}}(\boldsymbol{x}_k,l)\big)\,s_{k|k-1}^{(l)}(\boldsymbol{x}_k)\,\mathrm{d}\boldsymbol{x}_k$. Thus, the existence of the object with label l is uncertain (as described by the existence probability $r_k^{(l,0)}$ in (25)). Note that $r_k^{(l,0)}=0$ would indicate that the labeled object with state $(\mathbf{x}_k,l)$ does not exist and $r_k^{(l,0)}=1$ would indicate that the object exists but does not generate a measurement. If the object exists, its state $(\mathbf{x}_k,l)$ is distributed according to $s_k^{(l,0)}(\boldsymbol{x}_k)$ in (26). The plausibility of these events (i.e., that the labeled object with state $(\mathbf{x}_k,l)$ does not exist or it exists but does not generate a measurement) is quantified by $\beta_k^{(l,0)}$ in (24). Note that in the latter case, the labeled object with state $(\mathbf{x}_k,l)$ does not

generate a measurement in the current update step, but it did generate a measurement in a previous update step.

Finally, expressions of $\beta_k^{(m)}$, $\bar{r}_k^{(m)}$, and $\bar{s}_k^{(m)}(\boldsymbol{x}_k)$ for $m \in \mathcal{M}_k$ are given by [17]

$$\beta_k^{(m)} = \lambda_k^{\mathrm{C}}(\boldsymbol{z}_k^{(m)}) + d_k^{(m)}, \tag{27}$$

$$\bar{r}_k^{(m)} = \frac{d_k^{(m)}}{\beta_k^{(m)}}, \tag{28}$$

$$\bar{s}_k^{(m)}(\boldsymbol{x}_k) = \frac{p_{\mathrm{D}}(\boldsymbol{x}_k)\, f\big(\boldsymbol{z}_k^{(m)} \big| \boldsymbol{x}_k\big)\, \lambda_{k|k-1}(\boldsymbol{x}_k)}{d_k^{(m)}}, \tag{29}$$

with $d_k^{(m)} \triangleq \int p_{\mathrm{D}}(\boldsymbol{x}_k) f\big(\boldsymbol{z}_k^{(m)} \big| \boldsymbol{x}_k\big) \lambda_{k|k-1}(\boldsymbol{x}_k) \mathrm{d}\boldsymbol{x}_k$. Here, $\lambda_{k|k-1}(\boldsymbol{x}_k)$ was calculated in the prediction step, see (16), and $\lambda_k^{\mathrm{C}}(\boldsymbol{z}_k^{(m)})$ is the clutter PHD introduced in Section III-B. Note that $\bar{r}_k^{(m)} = 1$ would indicate that measurement $\boldsymbol{z}_k^{(m)}$ originates from an unlabeled object; the state $\mathbf{x}_k$ of that object is distributed according to $\bar{s}_k^{(m)}(\boldsymbol{x}_k)$ in (29). On the other hand, $\bar{r}_k^{(m)} = 0$ would indicate that $\boldsymbol{z}_k^{(m)}$ originates from clutter. The plausibility of this event (i.e., that measurement $\boldsymbol{z}_k^{(m)}$ originates from an unlabeled object or from clutter) is quantified by $\beta_k^{(m)}$ in (27).

B. Expression of the pgfl of Undetected Objects

It remains to provide an expression of the pgfl of undetected objects, $\bar{G}_{\mathsf{X}_k}[h]$ in (17). (Recall that an undetected object is an unlabeled object that is unlikely to exist and did not generate a measurement in the current update step.) A derivation analogous to [17] yields the Poisson pgfl (see (3))

$$\bar{G}_{\mathsf{X}_k}[h] = P[h; \lambda_k], \tag{30}$$

with

$$\lambda_k(\boldsymbol{x}_k) = (1 - p_{\mathrm{D}}(\boldsymbol{x}_k))\, \lambda_{k|k-1}(\boldsymbol{x}_k). \tag{31}$$

We note that $\bar{G}_{\mathsf{X}_k}[h]$ represents objects that are unlikely to exist and are also undetected.

In summary, the exact update step transforms the predicted posterior pgfl $G_{\tilde{\mathsf{X}}_k,\mathsf{X}_k}[\tilde{h}, h|Z_{1:k-1}]$ in (12), which is approximately the product of an LMB pgfl and a Poisson pgfl, into the new posterior pgfl $G_{\tilde{\mathsf{X}}_k,\mathsf{X}_k}[\tilde{h}, h|Z_{1:k}]$, which, according to (17) and our discussion above, is the product of the LMB–MB mixture pgfl $G'_{\tilde{\mathsf{X}}_k,\mathsf{X}_k}[\tilde{h}, h]$ in (18), (19) and the Poisson pgfl $\bar{G}_{\mathsf{X}_k}[h]$ in (30). The exact update step also takes into account the detection of objects that are unlikely to exist. This is achieved by the MB pgfl $M_{\mathcal{M}_{\boldsymbol{a}_k}}\big[h; \bar{r}_k^{(\cdot)}, \bar{s}_k^{(\cdot)}\big]$ involved in (18), which comprises one Bernoulli component for each observed measurement.

VI. Update Step of the LMB/P Filter: First Approximation Stage

The proposed LMB/P filter is now obtained by two successive approximations of the exact update step discussed above, which result in a significant reduction of complexity. The first approximation stage results in a transformation of certain unlabeled objects into labeled objects. More concretely, to reduce the complexity of data association, we first cluster the LMB–MB mixture pgfl $G'_{\tilde{\mathsf{X}}_k,\mathsf{X}_k}[\tilde{h}, h]$ in (19) into C LMB–MB mixture pgfls. Then we transfer unlabeled objects that were previously unlikely to exist but satisfy a suitable threshold criterion to the labeled object part, which means that they are now considered as objects that are likely to exist.

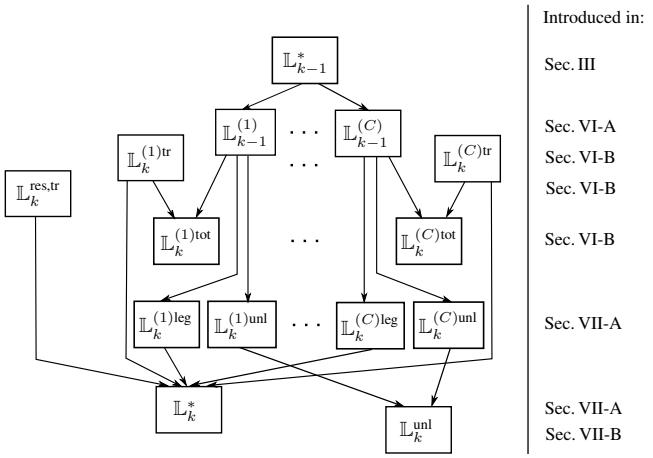

Fig. 1: Overview of the label sets involved in the approximations described in Sections VI and VII.

A. Partitioning of Label and Measurement Sets

The clustering of $G'_{\tilde{\mathsf{X}}_k,\mathsf{X}_k}[\tilde{h}, h]$ is based on a partitioning of the label set $\mathbb{L}_{k-1}^{*}$ and of the measurement index set $\mathcal{M}_k = \{1, \ldots, M_k\}$. We partition the label set $\mathbb{L}_{k-1}^{*}$ into $C \in \mathbb{N}$ disjoint subsets, i.e.,

$$\mathbb{L}_{k-1}^{*} = \bigcup_{c \in \mathcal{C}} \mathbb{L}_{k-1}^{(c)}, \tag{32}$$

where $\mathcal{C} \triangleq \{1, \ldots, C\}$, and we partition the measurement index set $\mathcal{M}_k$ into $C+1$ disjoint subsets, i.e.,

$$\mathcal{M}_k = \left(\bigcup_{c \in \mathcal{C}} \mathcal{M}_k^{(c)} \right) \cup \mathcal{M}_k^{\mathrm{res}}. \tag{33}$$

Each measurement index subset $\mathcal{M}_k^{(c)} \subseteq \mathcal{M}_k$ is associated with a corresponding label subset $\mathbb{L}_{k-1}^{(c)} \subseteq \mathbb{L}_{k-1}^{*}$, whereas the residual measurement index subset $\mathcal{M}_k^{\mathrm{res}} = \mathcal{M}_k \setminus \bigcup_{c \in \mathcal{C}} \mathcal{M}_k^{(c)}$ is not associated with any label set. More specifically, the partitionings (32) and (33) are chosen such that for any $c \in \mathcal{C}$, the association (described by $a_k^{(l)}$) of an object with state $(\mathbf{x}_k, l)$, $l \in \mathbb{L}_{k-1}^{(c)}$ with a measurement with index m is plausible for $m \in \mathcal{M}_k^{(c)}$ and implausible for $m \in \mathcal{M}_k^{(c')}$ with $c' \neq c$. Here, the plausibility of an association is quantified by the association weight $\beta_k^{(l,m)}$ in (21). An algorithm for constructing the partitionings (32) and (33) is presented in Appendix A. This algorithm uses a nonnegative threshold γ_{C} that determines $\mathbb{L}_{k-1}^{(c)}$, $\mathcal{M}_k^{(c)}$, and $\mathcal{M}_k^{\mathrm{res}}$.

The partitionings of $\mathbb{L}_{k-1}^{*}$ and $\mathcal{M}_k$ are illustrated in Fig. 1 and Fig. 2, respectively. The overall partitioning scheme is similar in spirit to the classical gating procedure used, e.g., in the joint probabilistic data association filter [1]. However, it is different in that it considers also the (non)existence of objects,

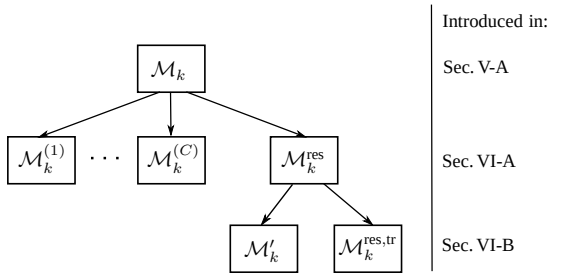

Fig. 2: Overview of the measurement index sets involved in the approximations described in Sections VI and VII.

it uses the association weights $\beta_k^{(l,m)}$ as plausibility measures, and it collects all the residual measurement indices in $\mathcal{M}_k^{\text{res}}$.

B. Approximation of the pgfls of Detected and Undetected Objects

Based on the label and measurement partitionings described above, we approximate the posterior pgfl $G_{\tilde{\mathbf{X}}_k,\mathbf{X}_k}[\tilde{h},h|Z_{1:k}]$ in (17) according to

$$G_{\tilde{\mathbf{X}}_k,\mathbf{X}_k}[\tilde{h},h|Z_{1:k}] \approx G'_{\tilde{\mathbf{X}}_k}[\tilde{h}]\,G'_{\mathbf{X}_k}[h], \tag{34}$$

where expressions of the factors $G'_{\tilde{\mathbf{X}}_k}[\tilde{h}]$ and $G'_{\mathbf{X}_k}[h]$ will be provided presently. As mentioned earlier, this approximation involves the clustering of the LMB-MB mixture pgfl $G_{\tilde{\mathbf{X}}_k,\mathbf{X}_k}[\tilde{h},h|Z_{1:k}]$ into C LMB-MB mixture pgfls and the transfer of certain unlabeled objects to labeled objects. The clustering step combined with the pruning of implausible association hypotheses significantly reduces the complexity of data association. The transfer step implicates that unlabeled objects that are likely to exist are now modeled by the labeled object part. A detailed description of the clustering and transfer steps is provided in Appendix B. Most of the pgfls involved in the approximations described in Sections VI and VII and in Appendix B are illustrated in Fig. 3.

Labeled pgfl factor: The labeled pgfl factor $G'_{\tilde{\mathbf{X}}_k}[\tilde{h}]$ in (34) represents objects that are likely to exist; it is given by

$$G'_{\tilde{\mathbf{X}}_k}[\tilde{h}] \triangleq L_{\mathbb{L}_k^{\text{res,tr}}}\big[\tilde{h};\bar{r}_k^{(\cdot)},\bar{s}_k^{(\cdot)}\big]\prod_{c\in\mathcal{C}} G^{(c)}[\tilde{h}]. \tag{35}$$

Here, according to the derivation described in Appendix B.3, the labeled objects represented by the LMB pgfl $L_{\mathbb{L}_k^{\text{res,tr}}}\big[\tilde{h};\bar{r}_k^{(\cdot)},\bar{s}_k^{(\cdot)}\big]$ include objects that were transferred from the set of unlabeled objects. The label set $\mathbb{L}_k^{\text{res,tr}}$ consists of all labels $l=(k,m)$ with $m\in\mathcal{M}_k^{\text{res,tr}}$, where $\mathcal{M}_k^{\text{res,tr}}\subseteq\mathcal{M}_k^{\text{res}}$ comprises all $m\in\mathcal{M}_k^{\text{res}}$ for which $\bar{r}_k^{(m)}\geq\gamma_{\text{tr}}$, with γ_{tr} being a positive threshold. Furthermore, $\bar{r}_k^{(m)}$ and $\bar{s}^{(m)}(\boldsymbol{x}_k)$ are given by (28) and (29), respectively.

The factors $G^{(c)}[\tilde{h}]$ in (35), just as the factor $L_{\mathbb{L}_k^{\text{res,tr}}}\big[\tilde{h};\bar{r}_k^{(\cdot)},\bar{s}_k^{(\cdot)}\big]$, represent labeled objects that are likely to exist. As described in Appendix B.2, some of these objects were transferred from the set of unlabeled objects within the respective cluster c. The underlying clustering step, described in Appendix B.1, significantly reduces the complexity of data association. For an expression of the

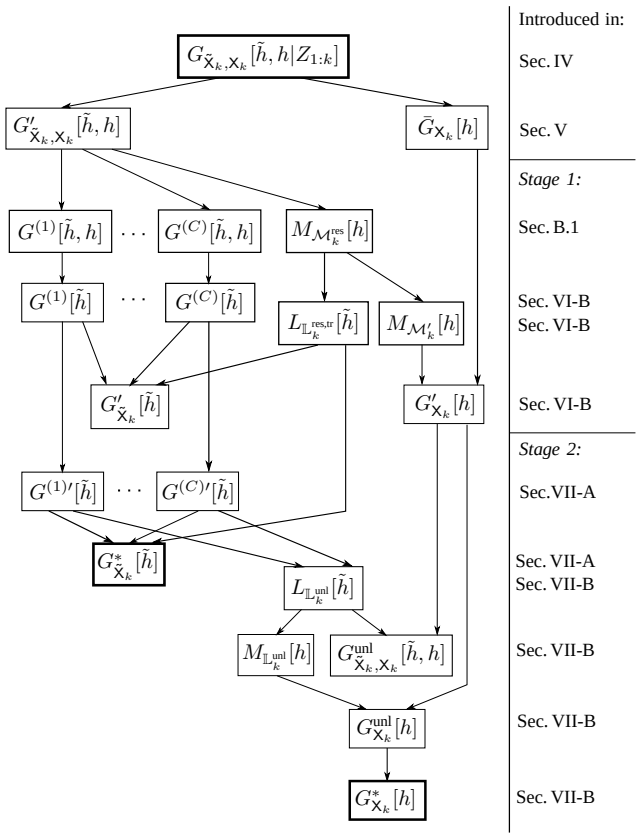

Fig. 3: Overview of some of the pgfls involved in the approximations described in Sections VI and VII and in Appendix B. For simplicity of notation, we omit the existence probabilities and spatial pdfs in the pgfls; e.g., we write $M_{\mathcal{M}_k^{\text{res}}}[h]$ instead of $M_{\mathcal{M}_k^{\text{res}}}\big[h;\bar{r}_k^{(\cdot)},\bar{s}_k^{(\cdot)}\big]$.

factors $G^{(c)}[\tilde{h}]$, we first introduce the random association vectors $\mathbf{a}_k^{(c)}\in\tilde{\mathcal{A}}_k^{(c)}\triangleq\big(\{0\}\cup\mathcal{M}_k^{(c)}\big)^{|\mathbb{L}_{k-1}^{(c)}|}\times\{0,1\}^{|\mathbb{L}_k^{(c)\text{tr}}|}$, where the entries $a_k^{(c,l)}$ of a realization $\boldsymbol{a}_k^{(c)}$ are as follows. For $l\in\mathbb{L}_{k-1}^{(c)}$, $a_k^{(c,l)}$ is defined similarly to $a_k^{(l)}$ in Section V-A as $a_k^{(c,l)}\triangleq m\in\mathcal{M}_k^{(c)}$ if the labeled object with state $(\mathbf{x}_k,l)$ generates measurement $\boldsymbol{z}_k^{(m)}$ and $a_k^{(c,l)}\triangleq 0$ if it does not generate a measurement. For $l\in\mathbb{L}_k^{(c)\text{tr}}$, $a_k^{(c,l)}$ is 1 if the labeled object with state $(\mathbf{x}_k,l)$ with $l=(k,m)$, $m\in\mathcal{M}_k^{(c)}$ generates measurement $\boldsymbol{z}_k^{(m)}$ and 0 if it does not generate a measurement. Similarly to Section V-A, we call $\boldsymbol{a}_k^{(c)}$ admissible if at most one measurement is assigned to a labeled object and no measurement is assigned to more than one labeled object. The set $\mathcal{A}_k^{(c)}\subseteq\tilde{\mathcal{A}}_k^{(c)}$ collects all admissible association vectors $\boldsymbol{a}_k^{(c)}$.

The factors $G^{(c)}[\tilde{h}]$ in (35) are LMBM pgfls given by

$$G^{(c)}[\tilde{h}] \triangleq \sum_{\boldsymbol{a}_k^{(c)}\in\mathcal{A}_k^{(c)}} w_{\boldsymbol{a}_k^{(c)}}\,L_{\mathbb{L}_k^{(c)\text{tot}}}\big[\tilde{h};r_k^{(\cdot,a_k^{(c,\cdot)})},s_k^{(\cdot,a_k^{(c,\cdot)})}\big]. \tag{36}$$

Here, the label set $\mathbb{L}_k^{(c)\text{tot}}$ is given as (see Fig. 1)

$$\mathbb{L}_k^{(c)\text{tot}}\triangleq\mathbb{L}_{k-1}^{(c)}\cup\mathbb{L}_k^{(c)\text{tr}},\quad\text{with }\mathbb{L}_{k-1}^{(c)}\cap\mathbb{L}_k^{(c)\text{tr}}=\emptyset, \tag{37}$$

where the label set $\mathbb{L}_k^{(c)\text{tr}}$ consists of all labels $l=(k,m)$ with $m\in\mathcal{M}_k^{(c)}$ such that $\bar{r}_k^{(m)}\geq\gamma_{\text{tr}}$. Furthermore, $r_k^{(l,m)}$ and $s_k^{(l,m)}(\boldsymbol{x}_k)$ are as follows. For $l\in\mathbb{L}_{k-1}^{(c)}$, they are given for

$m \in \mathcal{M}_k^{(c)}$ by (22) and (23), respectively and for $m=0$ by (25) and (26), respectively. For $l \in \mathbb{L}_k^{(c)\mathrm{tr}}$, $r_k^{(l,1)}$ and $s_k^{(l,1)}(\boldsymbol{x}_k)$ with $l=(k,m)$, $m \in \mathcal{M}_k^{(c)}$ are given by (28) and (29), respectively; furthermore, $r_k^{(l,0)}=0$ whereas $s_k^{(l,0)}(\boldsymbol{x}_k)$ is not defined since the corresponding object does not exist. Finally, the weights $w_{\boldsymbol{a}_k^{(c)}}$ are given up to a normalization constant as

$$w_{\boldsymbol{a}_k^{(c)}} \propto \Bigg(\prod_{l \in \mathbb{L}_k^{(c)\mathrm{tot}}} \beta_k^{(l,a_k^{(c,l)})} \Bigg) \prod_{m \in \mathcal{M}_{\boldsymbol{a}_k^{(c)}}} \beta_k^{(m)}, \tag{38}$$

where $\mathcal{M}_{\boldsymbol{a}_k^{(c)}} \subseteq \mathcal{M}_k^{(c)}$ comprises all $m \in \mathcal{M}_k^{(c)}$ that are not associated with any object label $l \in \mathbb{L}_k^{(c)\mathrm{tot}}$. For $l \in \mathbb{L}_{k-1}^{(c)}$, the association weights $\beta_k^{(l,m)}$ are given for $m \in \mathcal{M}_k^{(c)}$ by (21) and for $m=0$ by (24), and for $l \in \mathbb{L}_k^{(c)\mathrm{tr}}$, the $\beta_k^{(l,m)}$ are given for $m=1$ by (27) and for $m=0$ by 1. Furthermore, the $\beta_k^{(m)}$ are given by (27).

Unlabeled pgfl factor: The unlabeled pgfl factor $G'_{\mathsf{X}_k}[h]$ in (34) represents unlabeled objects that are unlikely to exist; it is given by

$$G'_{\mathsf{X}_k}[h] \triangleq M_{\mathcal{M}'_k}\big[h; \bar{r}_k^{(\cdot)}, \bar{s}_k^{(\cdot)}\big]\, \bar{G}_{\mathsf{X}_k}[h]. \tag{39}$$

Here, $\mathcal{M}'_k \triangleq \mathcal{M}_k^{\mathrm{res}} \setminus \mathcal{M}_k^{\mathrm{res,tr}}$, and $\bar{r}_k^{(m)}$ and $\bar{s}_k^{(m)}(\boldsymbol{x}_k)$ are given by (28) and (29), respectively. Furthermore, $\bar{G}_{\mathsf{X}_k}[h]$ is the Poisson pgfl given by (30) and (31). Thus, $G'_{\mathsf{X}_k}[h]$ is an MB–Poisson pgfl.

Summary of the first approximation stage: In summary, in the first approximation stage, the exact posterior pgfl $G_{\tilde{\mathsf{X}}_k,\mathsf{X}_k}[\tilde{h},h|Z_{1:k}]$ in (17), which is the product of the labeled/unlabeled pgfl $G'_{\tilde{\mathsf{X}}_k,\mathsf{X}_k}[\tilde{h},h]$ and the unlabeled pgfl $\bar{G}_{\mathsf{X}_k}[h]$, is approximated by $G'_{\tilde{\mathsf{X}}_k}[\tilde{h}]\,G'_{\mathsf{X}_k}[h]$ in (34). Here, the factor $G'_{\tilde{\mathsf{X}}_k}[\tilde{h}]$ is the pgfl of a labeled RFS representing objects that are likely to exist. More specifically, it is the product of the LMB pgfl $L_{\mathbb{L}_k^{\mathrm{res,tr}}}\big[\tilde{h}; \bar{r}_k^{(\cdot)}, \bar{s}_k^{(\cdot)}\big]$ and the LMBM pgfls $G^{(c)}[\tilde{h}]$, $c=1,\ldots,C$. The other factor, $G'_{\mathsf{X}_k}[h]$, is the pgfl of an unlabeled RFS representing objects that are unlikely to exist. More specifically, it is the product of the MB pgfl $M_{\mathcal{M}'_k}\big[h; \bar{r}_k^{(\cdot)}, \bar{s}_k^{(\cdot)}\big]$ and the Poisson pgfl $\bar{G}_{\mathsf{X}_k}[h]$. The effect of the first approximation stage is to reduce the overall complexity (based on the clustering described in Section VI-A) and to transfer the part of the unlabeled RFS representing likely unlabeled objects to the labeled RFS (as described in Appendices B.2 and B.3). Note that the resulting creation of new labeled objects is an inherent part of our tracking algorithm, and not due to a birth process in our system model (cf. Section III-A).

VII. Update Step of the LMB/P Filter: Second Approximation Stage

In the second approximation stage, we approximate $G'_{\tilde{\mathsf{X}}_k}[\tilde{h}]$ in (34) and (35), which is the product of an LMB pgfl and C LMBM pgfls, by an LMB pgfl. Furthermore, we modify $G'_{\mathsf{X}_k}[h]$ in (34) and (39), which is the product of an MB pgfl and a Poisson pgfl. This modification consists of first combining $G'_{\mathsf{X}_k}[h]$ with the "unlikely" legacy Bernoulli components of the LMB pgfl approximating $G'_{\tilde{\mathsf{X}}_k}[\tilde{h}]$ and then approximating the resulting pgfl by a Poisson pgfl.

A. Labeled Objects

We first approximate the pgfl of labeled objects, $G'_{\tilde{\mathsf{X}}_k}[\tilde{h}]$, by an LMB pgfl, and then we transfer labeled objects that are unlikely to exist to the unlabeled RFS part. This transfer is known as recycling [18].

According to (35), the pgfl of labeled objects $G'_{\tilde{\mathsf{X}}_k}[\tilde{h}]$ is the product of the pgfl representing objects transferred from the set of unlabeled nonclustered objects, $L_{\mathbb{L}_k^{\mathrm{res,tr}}}\big[\tilde{h}; \bar{r}_k^{(\cdot)}, \bar{s}_k^{(\cdot)}\big]$, and the product of all C pgfls $G^{(c)}[\tilde{h}]$ representing labeled clustered objects. To approximate $G'_{\tilde{\mathsf{X}}_k}[\tilde{h}]$ by an LMB pgfl, we first note that the product of LMB pgfls is again an LMB pgfl, and that $L_{\mathbb{L}_k^{\mathrm{res,tr}}}\big[\tilde{h}; \bar{r}_k^{(\cdot)}, \bar{s}_k^{(\cdot)}\big]$ is already an LMB pgfl. Therefore, we will approximate the LMBM pgfls $G^{(c)}[\tilde{h}]$, $c \in \mathcal{C}$ by LMB pgfls. For this, we start from expression (36) and exploit the fact that the weights $w_{\boldsymbol{a}_k^{(c)}}$, $\boldsymbol{a}_k^{(c)} \in \mathcal{A}_k^{(c)}$ in (38) satisfy $\sum_{\boldsymbol{a}_k^{(c)} \in \mathcal{A}_k^{(c)}} w_{\boldsymbol{a}_k^{(c)}} = 1$. Thus, we are able to formally interpret these weights as the pmf of the joint association vector $\mathbf{a}_k^{(c)}$, i.e., we set

$$p\big(\boldsymbol{a}_k^{(c)}\big) \triangleq \begin{cases} w_{\boldsymbol{a}_k^{(c)}}, & \boldsymbol{a}_k^{(c)} \in \mathcal{A}_k^{(c)}, \\ 0, & \text{otherwise.} \end{cases} \tag{40}$$

Expression (36) can then be rewritten as

$$G^{(c)}[\tilde{h}] = \sum_{\boldsymbol{a}_k^{(c)} \in \tilde{\mathcal{A}}_k^{(c)}} p\big(\boldsymbol{a}_k^{(c)}\big)\, L_{\mathbb{L}_k^{(c)\mathrm{tot}}}\big[\tilde{h}; r_k^{(\cdot,a_k^{(c,\cdot)})}, s_k^{(\cdot,a_k^{(c,\cdot)})}\big]. \tag{41}$$

Note that the summation over the larger set $\tilde{\mathcal{A}}_k^{(c)} = \big(\{0\} \cup \mathcal{M}_k^{(c)}\big)^{|\mathbb{L}_{k-1}^{(c)}|} \times \{0,1\}^{|\mathbb{L}_k^{(c)\mathrm{tr}}|}$ (i.e., larger than $\mathcal{A}_k^{(c)}$ in (36)) is possible because $p\big(\boldsymbol{a}_k^{(c)}\big)=0$ for $\boldsymbol{a}_k^{(c)} \in \tilde{\mathcal{A}}_k^{(c)} \setminus \mathcal{A}_k^{(c)}$.

Following [17], we now approximate $p\big(\boldsymbol{a}_k^{(c)}\big)$ by the product of the marginal pmfs $p\big(a_k^{(c,l)}\big)$, i.e.,

$$p\big(\boldsymbol{a}_k^{(c)}\big) \approx p'\big(\boldsymbol{a}_k^{(c)}\big) \triangleq \prod_{l \in \mathbb{L}_k^{(c)\mathrm{tot}}} p\big(a_k^{(c,l)}\big), \quad \boldsymbol{a}_k^{(c)} \in \tilde{\mathcal{A}}_k^{(c)}.$$

Here,

$$p\big(a_k^{(c,l)}\big) \triangleq \begin{cases} \sum_{\boldsymbol{a}_k^{(c)\sim l} \in \tilde{\mathcal{A}}_k^{(c)\mathrm{leg}}} p\big(\boldsymbol{a}_k^{(c)}\big), & l \in \mathbb{L}_{k-1}^{(c)}, \\ \sum_{\boldsymbol{a}_k^{(c)\sim l} \in \tilde{\mathcal{A}}_k^{(c)\mathrm{tr}}} p\big(\boldsymbol{a}_k^{(c)}\big), & l \in \mathbb{L}_k^{(c)\mathrm{tr}} \end{cases} \tag{42}$$

(recall from (37) that $\mathbb{L}_k^{(c)\mathrm{tot}} = \mathbb{L}_{k-1}^{(c)} \cup \mathbb{L}_k^{(c)\mathrm{tr}}$), where $\boldsymbol{a}_k^{(c)\sim l}$ denotes $\boldsymbol{a}_k^{(c)}$ without entry $a_k^{(c,l)}$, $\tilde{\mathcal{A}}_k^{(c)\mathrm{leg}} \triangleq \big(\{0\} \cup \mathcal{M}_k^{(c)}\big)^{|\mathbb{L}_{k-1}^{(c)}|-1} \times \{0,1\}^{|\mathbb{L}_k^{(c)\mathrm{tr}}|}$, and $\tilde{\mathcal{A}}_k^{(c)\mathrm{tr}} \triangleq \big(\{0\} \cup \mathcal{M}_k^{(c)}\big)^{|\mathbb{L}_{k-1}^{(c)}|} \times \{0,1\}^{|\mathbb{L}_k^{(c)\mathrm{tr}}|-1}$. We note that an efficient and scalable approximate implementation of the marginalization in (42) is provided by the belief propagation algorithm proposed in [17]. Substituting $p'\big(\boldsymbol{a}_k^{(c)}\big)$ for $p\big(\boldsymbol{a}_k^{(c)}\big)$ in (41) and using the fact that the LMB pgfl $L_{\mathbb{L}_k^{(c)\mathrm{tot}}}\big[\tilde{h}; r_k^{(\cdot,a_k^{(c,\cdot)})}, s_k^{(\cdot,a_k^{(c,\cdot)})}\big]$ representing all (labeled) objects within cluster c is the product of all corresponding labeled Bernoulli pgfls $B\big[\tilde{h}; r_k^{(l,a_k^{(c,l)})}, s_k^{(l,a_k^{(c,l)})}\big]$ (see (8)), we obtain the following approximation of $G^{(c)}[\tilde{h}]$:

$$G^{(c)\prime}[\tilde{h}] \triangleq \sum_{\boldsymbol{a}_k^{(c)} \in \tilde{\mathcal{A}}_k^{(c)}} \prod_{l \in \mathbb{L}_k^{(c)\mathrm{tot}}} p\big(a_k^{(c,l)}\big)\, B\big[\tilde{h}; r_k^{(l,a_k^{(c,l)})}, s_k^{(l,a_k^{(c,l)})}\big].$$

Using the identities $\prod_{l\in\mathbb{L}_k^{(c)\text{tot}}} = \Big(\prod_{l\in\mathbb{L}_{k-1}^{(c)}}\Big)\prod_{l\in\mathbb{L}_k^{(c)\text{tr}}}$ and

$$\sum_{\boldsymbol{a}_k^{(c)}\in\tilde{\mathcal{A}}_k^{(c)}} = \sum_{a_k^{(c,1)}\in\{0\}\cup\mathcal{M}_k^{(c)}} \cdots \sum_{a_k^{(c,|\mathbb{L}_{k-1}^{(c)}|)}\in\{0\}\cup\mathcal{M}_k^{(c)}} \times \sum_{a_k^{(c,|\mathbb{L}_{k-1}^{(c)}|+1)}\in\{0,1\}} \cdots \sum_{a_k^{(c,|\mathbb{L}_{k-1}^{(c)}|+|\mathbb{L}_k^{(c)\text{tr}}|)}\in\{0,1\}},$$

this becomes

$$\begin{aligned} &G^{(c)\prime}[\tilde{h}] \\ &= \Bigg(\prod_{l\in\mathbb{L}_{k-1}^{(c)}} \sum_{a_k^{(c,l)}\in\{0\}\cup\mathcal{M}_k^{(c)}} p\big(a_k^{(c,l)}\big)\, B\big[\tilde{h}; r_k^{(l,a_k^{(c,l)})}, s_k^{(l,a_k^{(c,l)})}\big]\Bigg) \\ &\quad\times \prod_{l\in\mathbb{L}_k^{(c)\text{tr}}} \sum_{a_k^{(c,l)}\in\{0,1\}} p\big(a_k^{(c,l)}\big)\, B\big[\tilde{h}; r_k^{(l,a_k^{(c,l)})}, s_k^{(l,a_k^{(c,l)})}\big]. \end{aligned}$$

Using (5), this can be written as the LMB pgfl

$$G^{(c)\prime}[\tilde{h}] = L_{\mathbb{L}_k^{(c)\text{tot}}}\big[\tilde{h}; r_k^{(\cdot)}, s_k^{(\cdot)}\big], \tag{43}$$

where, according to (6), $r_k^{(l)}$ and $s_k^{(l)}(\boldsymbol{x}_k)$ are given for $l\in\mathbb{L}_{k-1}^{(c)}$ by

$$r_k^{(l)} = \sum_{a_k^{(c,l)}\in\{0\}\cup\mathcal{M}_k^{(c)}} p\big(a_k^{(c,l)}\big)\, r_k^{(l,a_k^{(c,l)})}, \tag{44}$$

$$s_k^{(l)}(\boldsymbol{x}_k) = \frac{1}{r_k^{(l)}} \sum_{a_k^{(c,l)}\in\{0\}\cup\mathcal{M}_k^{(c)}} p\big(a_k^{(c,l)}\big)\, r_k^{(l,a_k^{(c,l)})}\, s_k^{(l,a_k^{(c,l)})}(\boldsymbol{x}_k), \tag{45}$$

and for $l\in\mathbb{L}_k^{(c)\text{tr}}$ by

$$r_k^{(l)} = p\big(a_k^{(c,l)}=1\big)\, r_k^{(l,a_k^{(c,l)}=1)}, \tag{46}$$

$$s_k^{(l)}(\boldsymbol{x}_k) = s_k^{(l,a_k^{(c,l)}=1)}(\boldsymbol{x}_k). \tag{47}$$

(To obtain (46) and (47), we used the fact that $r_k^{(l,a_k^{(c,l)}=0)}=0$ for $l\in\mathbb{L}_k^{(c)\text{tr}}$, as mentioned in Section VI-B.) Note that (44)–(47) are update equations for the labeled objects; more specifically, (44) and (45) for the legacy Bernoulli components and (46) and (47) for the transferred Bernoulli components. It can be shown that our LMB approximation of the LMBM pgfls—which is based on interpreting the weights $w_{\boldsymbol{a}_k^{(c)}}$ as the joint association pmf $p\big(\boldsymbol{a}_k^{(c)}\big)$ and approximating that pmf by the product of its marginals—is equivalent to the LMB approximation of the LMBM pgfls that is obtained by matching the PHD of each LMB pgfl to that of the corresponding LMBM pgfl (similarly to [11]).

Let $\mathbb{L}_k^{(c)\text{leg}}\subseteq\mathbb{L}_{k-1}^{(c)}$ collect the labels $l\in\mathbb{L}_{k-1}^{(c)}$ of those legacy Bernoulli components that are "likely" in the sense that their existence probability $r_k^{(l)}$ in (44) satisfies $r_k^{(l)}\geq\gamma_{\text{leg}}$, where γ_{leg} is another positive threshold. The total label set of all "likely" legacy Bernoulli components and transferred Bernoulli components is then given by (see Fig. 1)

$$\mathbb{L}_k^{*} \triangleq \Bigg(\bigcup_{c\in\mathcal{C}}\big(\mathbb{L}_k^{(c)\text{leg}}\cup\mathbb{L}_k^{(c)\text{tr}}\big)\Bigg)\cup\mathbb{L}_k^{\text{res,tr}}, \tag{48}$$

where $\mathbb{L}_k^{\text{res,tr}}$ was introduced in Section VI-B. The LMB pgfl corresponding to $\mathbb{L}_k^{*}$ is now given by

$$\begin{aligned} G_{\tilde{\mathsf{X}}_k}^{*}[\tilde{h}] &\triangleq L_{\mathbb{L}_k^{*}}\big[\tilde{h}; r_k^{(\cdot)}, s_k^{(\cdot)}\big] \\ &= L_{\mathbb{L}_k^{\text{res,tr}}}\big[\tilde{h}; \bar{r}_k^{(\cdot)}, \bar{s}_k^{(\cdot)}\big] \prod_{c\in\mathcal{C}} L_{\mathbb{L}_k^{(c)\text{leg}}\cup\mathbb{L}_k^{(c)\text{tr}}}\big[\tilde{h}; r_k^{(\cdot)}, s_k^{(\cdot)}\big] \end{aligned} \tag{49}$$

(see Fig. 3). According to (49), $G_{\tilde{\mathsf{X}}_k}^{*}[\tilde{h}]$ equals the product of the LMB pgfl $L_{\mathbb{L}_k^{\text{res,tr}}}\big[\tilde{h}; \bar{r}_k^{(\cdot)}, \bar{s}_k^{(\cdot)}\big]$ involved in (35) and the C LMB pgfls obtained by restricting the LMB pgfls in (43) to the label sets $\mathbb{L}_k^{(c)\text{leg}}\cup\mathbb{L}_k^{(c)\text{tr}}$, for all $c\in\mathcal{C}$. This is our final approximation of the labeled object part, i.e., of the pgfl $G'_{\tilde{\mathsf{X}}_k}[\tilde{h}]$ in (35). That is, we have

$$G'_{\tilde{\mathsf{X}}_k}[\tilde{h}] \approx G_{\tilde{\mathsf{X}}_k}^{*}[\tilde{h}].$$

The "unlikely" legacy Bernoulli components correspond to the labels $l\in\mathbb{L}_{k-1}^{(c)}$ with $r_k^{(l)}<\gamma_{\text{leg}}$, or equivalently $l\in\mathbb{L}_k^{(c)\text{unl}} \triangleq \mathbb{L}_{k-1}^{(c)}\setminus\mathbb{L}_k^{(c)\text{leg}}$. Instead of discarding them, as is done, e.g., in the LMB filter [11], we use recycling [18], i.e., we transfer them to the unlabeled RFS part. As a consequence, these unlikely objects are still being tracked but with a smaller computational cost. A higher threshold γ_{leg} tends to imply that fewer Bernoulli components remain in the labeled RFS part and more are transferred to the unlabeled RFS part. In particular, when many measurements are missing (due to, e.g., object death or object occlusion), then $r_k^{(l)}$ is decreased, and if $r_k^{(l)}<\gamma_{\text{leg}}$, then the corresponding labeled Bernoulli component will be transferred to the unlabeled RFS part. We note that the Bernoulli components transferred to the unlabeled RFS part comprise only *legacy* Bernoulli components and do not include Bernoulli components that were transferred from the unlabeled RFS part to the labeled RFS part in the current time step. This is due to the fact that the corresponding label sets $\mathbb{L}_{k-1}^{(c)}$ and $\mathbb{L}_k^{(c)\text{tr}}$ are disjoint (cf. (37)) and, thus, Bernoulli components that were transferred from the unlabeled RFS part to the labeled RFS part are not transferred back in the current time step.

B. Unlabeled Objects

We proceed by representing unlabeled and currently labeled objects that are unlikely to exist by a Poisson RFS. Compared to our previous use of an LMB RFS to represent objects that are likely to exist, using a Poisson RFS reduces the computational complexity at the expense of a decreased tracking accuracy and the loss of track continuity for the respective objects.

Consider the unlikely legacy objects defined by the label set (see Fig. 1)

$$\mathbb{L}_k^{\text{unl}} \triangleq \bigcup_{c\in\mathcal{C}} \mathbb{L}_k^{(c)\text{unl}}. \tag{50}$$

The labeled pgfl comprising the corresponding Bernoulli components is given by $L_{\mathbb{L}_k^{\text{unl}}}\big[\tilde{h}; r_k^{(\cdot)}, s_k^{(\cdot)}\big]$ (see Fig. 3). We now combine this labeled pgfl with the unlabeled pgfl $G'_{\mathsf{X}_k}[h]$ in (39) by defining

$$G_{\tilde{\mathsf{X}}_k,\mathsf{X}_k}^{\text{unl}}[\tilde{h},h] \triangleq L_{\mathbb{L}_k^{\text{unl}}}\big[\tilde{h}; r_k^{(\cdot)}, s_k^{(\cdot)}\big]\, G'_{\mathsf{X}_k}[h]. \tag{51}$$

We recall that $G'_{\mathbf{X}_k}[h]$ is the product of an MB pgfl and a Poisson pgfl (see (39)), and it represents unlabeled objects that are unlikely. Thus, the LMB–MB–Poisson pgfl $G^{\text{unl}}_{\tilde{\mathbf{X}}_k,\mathbf{X}_k}[\tilde{h},h]$ represents the labeled and unlabeled objects that are unlikely.

To further reduce the complexity of the update step, we next approximate $G^{\text{unl}}_{\tilde{\mathbf{X}}_k,\mathbf{X}_k}[\tilde{h},h]$ by a Poisson pgfl, i.e. (see Fig. 3)

$$G^{\text{unl}}_{\tilde{\mathbf{X}}_k,\mathbf{X}_k}[\tilde{h},h] \approx G^{*}_{\mathbf{X}_k}[h] \triangleq P[h;\lambda^{*}_k]. \tag{52}$$

To find the PHD $\lambda^{*}_k(\boldsymbol{x}_k)$, we first "unlabel" the LMB pgfl $L_{\mathbb{L}^{\text{unl}}_k}\big[\tilde{h};r^{(\cdot)}_k,s^{(\cdot)}_k\big]$. This results in the MB pgfl $M_{\mathbb{L}^{\text{unl}}_k}\big[h;r^{(\cdot)}_k,s^{(\cdot)}_k\big]$, wherein $l\in\mathbb{L}^{\text{unl}}_k$ is used solely to index the Bernoulli components, and not as the label of a labeled state $(\mathbf{x}_k,l)$. Through this unlabeling, the mixed labeled/unlabeled (LMB–MB–Poisson) pgfl $G^{\text{unl}}_{\tilde{\mathbf{X}}_k,\mathbf{X}_k}[\tilde{h},h]$ in (51) is converted into the unlabeled (MB–Poisson) pgfl

$$G^{\text{unl}}_{\mathbf{X}_k}[h] \triangleq M_{\mathbb{L}^{\text{unl}}_k}\big[h;r^{(\cdot)}_k,s^{(\cdot)}_k\big]\,G'_{\mathbf{X}_k}[h].$$

The PHD $\lambda^{*}_k(\boldsymbol{x}_k)$ in (52) is now chosen as the PHD corresponding to $G^{\text{unl}}_{\mathbf{X}_k}[h]$. That is, invoking (2), we set $\lambda^{*}_k(\boldsymbol{x}_k)=\delta G^{\text{unl}}_{\mathbf{X}_k}[h]/\delta\boldsymbol{x}_k\big|_{h=1}$. Using (39), (30), and (31), this can be shown to yield

$$\begin{aligned}\lambda^{*}_k(\boldsymbol{x}_k) = &\sum_{l\in\mathbb{L}^{\text{unl}}_k} r^{(l)}_k s^{(l)}_k(\boldsymbol{x}_k) + \sum_{m\in\mathcal{M}'_k} \bar{r}^{(m)}_k \bar{s}^{(m)}_k(\boldsymbol{x}_k)\\ &+\big(1-p_{\text{D}}(\boldsymbol{x}_k)\big)\lambda_{k|k-1}(\boldsymbol{x}_k),\end{aligned} \tag{53}$$

where $r^{(l)}_k$ and $s^{(l)}_k(\boldsymbol{x}_k)$ are given by (44) and (45), respectively, $\bar{r}^{(m)}_k$ and $\bar{s}^{(m)}_k(\boldsymbol{x}_k)$ are given by (28) and (29), respectively, and $\lambda_{k|k-1}(\boldsymbol{x}_k)$ is given by (16). The first term in (53), $\sum_{l\in\mathbb{L}^{\text{unl}}_k} r^{(l)}_k s^{(l)}_k(\boldsymbol{x}_k)$, corresponds to originally labeled objects that are unlikely—either because the objects already disappeared or because no measurement was associated with them for some time. The second term, $\sum_{m\in\mathcal{M}'_k}\bar{r}^{(m)}_k\bar{s}^{(m)}_k(\boldsymbol{x}_k)$, corresponds to measurements that are not likely to originate from any labeled objects. The third term, $\big(1-p_{\text{D}}(\boldsymbol{x}_k)\big)\lambda_{k|k-1}(\boldsymbol{x}_k)$, corresponds to unlabeled objects that are undetected. The Poisson pgfl $G^{*}_{\mathbf{X}_k}[h]$ defined in (52) is our final approximation of the unlabeled object part.

VIII. The Proposed LMB/P Filter

The core of the proposed LMB/P filter algorithm is the approximate update step developed in Sections VI and VII. We recall that this approximate update step transforms the predicted posterior pgfl $G_{\tilde{\mathbf{X}}_k,\mathbf{X}_k}[\tilde{h},h|Z_{1:k-1}]$, which according to (12) is the product of the labeled pgfl $G^{\text{P}}_{\tilde{\mathbf{X}}_k}[\tilde{h}]$ and the unlabeled pgfl $G^{\text{P}}_{\mathbf{X}_k}[h]$, into the following approximation of the new posterior pgfl $G_{\tilde{\mathbf{X}}_k,\mathbf{X}_k}[\tilde{h},h|Z_{1:k}]$ in (17):

$$G_{\tilde{\mathbf{X}}_k,\mathbf{X}_k}[\tilde{h},h|Z_{1:k}] \approx G^{*}_{\tilde{\mathbf{X}}_k}[\tilde{h}]\,G^{*}_{\mathbf{X}_k}[h].$$

This is the product of the LMB pgfl $G^{*}_{\tilde{\mathbf{X}}_k}[\tilde{h}]$, which is given by (49) and (44)–(47), and the Poisson pgfl $G^{*}_{\mathbf{X}_k}[h]$, which is given by (52) and (53). The update relations are (44)–(47) for the LMB parameters (existence probabilities and spatial pdfs) and (53) for the Poisson parameter (PHD).

These update relations can be viewed as those of an LMB filter and a PHD filter that run in parallel but not independently of each other. The LMB part models objects that are likely to exist and uses in the update step measurements that are likely (plausible) to originate from these objects. It maintains track continuity of the modeled objects and offers a better tracking accuracy than the Poisson part. The Poisson part, on the other hand, models objects that are unlikely to exist, and it uses in the update step all those measurements that are unlikely (implausible) to originate from a labeled object and thus likely to originate from an unlabeled object or from clutter. Each measurement is used only once in the update step, either by the LMB part or by the Poisson part. The overall approximate update step includes transfers between the labeled and unlabeled RFS parts. That is, based on newly observed measurements, some objects that were previously considered unlikely to exist are considered likely to exist and vice versa. These transfers are controlled by the thresholds γ_{C}, γ_{tr}, and γ_{leg}.

The proposed LMB/P filter algorithm is finally obtained by cascading the prediction step (Section IV) and the approximate update step (Sections VI and VII), and by adding a detection-estimation step. Since the unlabeled RFS part represents objects that are unlikely to exist, object detection and state estimation are based solely on the labeled RFS part. An object with label $l\in\mathbb{L}^{*}_k$ is detected—i.e., declared to exist—if its existence probability $r^{(l)}_k$ is larger than a positive detection threshold γ_{D}; the label l is then included in the "detected label set" $\mathbb{L}^{\text{D}}_k\subseteq\mathbb{L}^{*}_k$. Subsequently, for each detected object $l\in\mathbb{L}^{\text{D}}_k$, a state estimate is calculated according to

$$\hat{\boldsymbol{x}}^{(l)}_k = \int \boldsymbol{x}_k\, s^{(l)}_k(\boldsymbol{x}_k)\,\mathrm{d}\boldsymbol{x}_k\,. \tag{54}$$

Table I summarizes the proposed LMB/P filter algorithm.

IX. Simulation Study

A. Simulation Setup

We evaluate the performance of the proposed LMB/P filter in two two-dimensional (2D) tracking scenarios, termed TS1 and TS2. In TS1, ten objects appear at randomly chosen positions in the region of interest (ROI) before time $k=40$ and disappear after $k=150$. In TS2, 20 objects appear before $k=100$ and disappear after $k=140$; they conform to the object generation scheme of [27], according to which all objects move toward the point $(0,0)$ and simultaneously come in close proximity around that point at $k=120$. The object states consist of 2D position and velocity, i.e. $\mathbf{x}_k=[\mathrm{x}_{1,k}\ \mathrm{x}_{2,k}\ \dot{\mathrm{x}}_{1,k}\ \dot{\mathrm{x}}_{2,k}]^{\text{T}}$. They evolve according to the nearly constant velocity motion model, i.e., $\mathbf{x}_k=\mathbf{A}\mathbf{x}_{k-1}+\mathbf{W}\mathbf{u}_k$, where $\mathbf{A}\in\mathbb{R}^{4\times4}$ and $\mathbf{W}\in\mathbb{R}^{4\times2}$ are chosen as in [28, Sec. 6.3.2] and $\mathbf{u}_k$ is an iid sequence of 2D zero-mean Gaussian random vectors with independent components and component variance $\sigma^2_u=10^{-4}$. The sensor is located at position $\boldsymbol{p}=[p_1\ p_2]^{\text{T}}=[0\ -50]^{\text{T}}$ and has a measurement range of 300. The ROI is equal to the disk determined by the sensor's measurement range. Realizations of the object trajectories for TS1 and TS2 are shown in Fig. 4.

The object-originated measurements conform to the nonlinear range-bearing model $\mathbf{z}_k=\big[\rho(\mathbf{x}_k)\ \theta(\mathbf{x}_k)\big]^{\text{T}}+\mathbf{v}_k$. Here, $\rho(\mathbf{x}_k)\triangleq\|\mathbf{x}'_k-\boldsymbol{p}\|$, where $\mathbf{x}'_k\triangleq[\mathrm{x}_{1,k}\ \mathrm{x}_{2,k}]^{\text{T}}$ is the object position, and $\theta(\mathbf{x}_k)\triangleq\tan^{-1}\big(\frac{\mathrm{x}_{2,k}-p_2}{\mathrm{x}_{1,k}-p_1}\big)$. Furthermore, $\mathbf{v}_k$ is 2D

TABLE I: Proposed LMB/P filter algorithm—recursion at time $k \geq 1$

Input: Previous existence probabilities $r_{k-1}^{(l)}$ and previous spatial pdfs $s_{k-1}^{(l)}(\boldsymbol{x}_{k-1})$ for $l \in \mathbb{L}_{k-1}^{*}$; previous PHD $\lambda_{k-1}(\boldsymbol{x}_{k-1})$ (in practice, this is replaced by the previously calculated approximation $\lambda_{k-1}^{*}(\boldsymbol{x}_{k-1})$); measurements $\boldsymbol{z}_k^{(m)}$ for $m \in \mathcal{M}_k$.

Output: Existence probabilities $r_k^{(l)}$ and spatial pdfs $s_k^{(l)}(\boldsymbol{x}_k)$ for $l \in \mathbb{L}_k^{*}$; approximate PHD $\lambda_k^{*}(\boldsymbol{x}_k)$; object state estimates $\hat{\boldsymbol{x}}_k^{(l)}$ for $l \in \mathbb{L}_k^{\mathrm{D}}$.

Operations:

Step 1 – Prediction:

1.1) For $l \in \mathbb{L}_{k-1}^{*}$, calculate the predicted existence probabilities $r_{k|k-1}^{(l)}$ and the predicted spatial pdfs $s_{k|k-1}^{(l)}(\boldsymbol{x}_k)$ according to (13) and (14), respectively.

1.2) Calculate the predicted posterior PHD $\lambda_{k|k-1}(\boldsymbol{x}_k)$ according to (16).

Step 2 – Preparations for Update:

2.1) For $l \in \mathbb{L}_{k-1}^{*}$, calculate the association weights $\beta_k^{(l,m)}$, existence probabilities $r_k^{(l,m)}$, and spatial pdfs $s_k^{(l,m)}(\boldsymbol{x}_k)$ according to (21)–(23) (for $m \in \mathcal{M}_k$) or (24)–(26) (for $m = 0$).

2.2) For $m \in \mathcal{M}_k$, calculate $\beta_k^{(m)}$, $\bar{r}_k^{(m)}$, and $\bar{s}_k^{(m)}(\boldsymbol{x}_k)$ according to (27)–(29).

2.3) Partition the label set $\mathbb{L}_{k-1}^{*}$ and the measurement index set $\mathcal{M}_k$ as described in Section VI-A. This yields $\mathbb{L}_{k-1}^{(c)}$ and $\mathcal{M}_k^{(c)}$ for $c \in \mathcal{C}$ as well as $\mathcal{M}_k^{\mathrm{res}}$.

2.4) Determine $\mathbb{L}_k^{(c)\mathrm{tr}}$ for $c \in \mathcal{C}$, $\mathbb{L}_k^{\mathrm{res,tr}}$ (corresponding to $\mathcal{M}_k^{\mathrm{res,tr}}$), and $\mathcal{M}_k'$ as described in Section VI-B.

Step 3 – Update for Labeled Objects:

3.1) For $c \in \mathcal{C}$, calculate the weights $w_{\boldsymbol{a}_k^{(c)}}$ according to (38) and the joint association pmf $p(\boldsymbol{a}_k^{(c)})$ according to (40).

3.2) For $c \in \mathcal{C}$ and $l \in \mathbb{L}_k^{(c)\mathrm{tot}} = \mathbb{L}_{k-1}^{(c)} \cup \mathbb{L}_k^{(c)\mathrm{tr}}$, calculate the marginal association pmf $p(a_k^{(c,l)})$ according to (42). (An efficient and scalable belief propagation algorithm for computing the $p(a_k^{(c,l)})$ is presented in [17].)

3.3) For $c \in \mathcal{C}$, calculate the updated existence probabilities $r_k^{(l)}$ and spatial pdfs $s_k^{(l)}(\boldsymbol{x}_k)$ according to (44) and (45) (for $l \in \mathbb{L}_{k-1}^{(c)}$) or (46) and (47) (for $l \in \mathbb{L}_k^{(c)\mathrm{tr}}$).

3.4) For $c \in \mathcal{C}$, determine $\mathbb{L}_k^{(c)\mathrm{leg}}$ and $\mathbb{L}_k^{(c)\mathrm{unl}}$ as described in Section VII-A.

3.5) Determine $\mathbb{L}_k^{*}$ according to (48) and $\mathbb{L}_k^{\mathrm{unl}}$ according to (50).

Step 4 – Update for Unlabeled Objects: Calculate the approximate updated posterior PHD $\lambda_k^{*}(\boldsymbol{x}_k)$ according to (53).

Step 5 – Object Detection and State Estimation:

5.1) Determine $\mathbb{L}_k^{\mathrm{D}}$ as described in Section VIII.

5.2) For $l \in \mathbb{L}_k^{\mathrm{D}}$, calculate an object state estimate $\hat{\boldsymbol{x}}_k^{(l)}$ according to (54).

Initialization at time $k = 0$**:** $\mathbb{L}_0^{*} = \emptyset$, $\lambda_0(\boldsymbol{x}_0)$.

zero-mean white Gaussian measurement noise with independent components and component standard deviations $\sigma_\rho = 2$ and $\sigma_\theta = 1^\circ$. The detection probability of the sensor is modeled as $p_{\mathrm{D}}(\boldsymbol{x}_k) = p_{\mathrm{D,max}} \exp(-\|\boldsymbol{x}_k'\|^2/450^2)$ [11] with $p_{\mathrm{D,max}} = 0.7$ for TS1 and $p_{\mathrm{D,max}} = 0.5$ for TS2. Thus, the detection probability has its maximum of 0.7 for TS1 and 0.5 for TS2 at the ROI center and decreases towards the ROI border, where it is

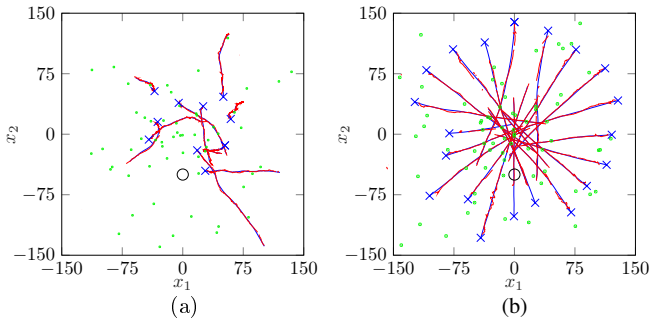

Fig. 4: Examples of the true object trajectories (represented by blue lines, starting positions indicated by blue crosses) and the corresponding estimates obtained with the proposed BP-LMB/P filter (represented by red lines) for (a) TS1 and (b) TS2. The position of the sensor is indicated by a black circle. The green circles show the measurements of the sensor at time $k = 100$ within the region $[-150, 150] \times [-150, 150]$.

0.45 for TS1 and 0.32 for TS2. The clutter pdf $f_{\mathrm{C}}(\boldsymbol{z}_k)$ is uniform (in polar coordinates) on the ROI with mean parameter $\mu_{\mathrm{C}} = 100$ for TS1 and $\mu_{\mathrm{C}} = 150$ for TS2.

We compare the performance of particle implementations of the proposed LMB/P filter, the LMB filter [12], the fast LMB filter presented in [13], and a version of the TOMB/P filter [17], [29] that performs recycling of Bernoulli components as proposed in [18]. We remark that our performance comparison does not consider algorithms with a significantly higher complexity, such as the GLMB filter [9], [10], [14] or the trajectory-based filters proposed in [21]–[24]. Note also that the latter filters use Gaussian representations of spatial distributions and thus presuppose a linear-Gaussian system model, and moreover they assume a spatially constant detection probability, both of which are incompatible with the considered measurement model. Our performance comparison uses 1,000 Monte Carlo runs for each experiment. The object trajectories are randomly generated for each run according to the state-evolution model described above.

The proposed LMB/P filter and the TOMB/P filter use the belief propagation (BP) algorithm of [17] to calculate approximations of the marginal association probabilities (cf. Eq. (42) and Step 3.2 in Table I), and the fast LMB filter uses for this task the modified BP algorithm described in [13]. We will therefore refer to these filters as BP-LMB/P, BP-TOMB/P, and BP-LMB, respectively. The LMB filter of [12] is based on the Gibbs sampler and will be referred to as Gibbs-LMB. BP-LMB/P and BP-TOMB/P use 5,000 particles to represent, respectively, the posterior PHD of unlabeled objects and the posterior PHD of undetected objects. Another 5,000 particles are used by BP-LMB/P and BP-TOMB/P to represent the PHD of newborn unlabeled objects and the PHD of newborn undetected objects, respectively, but the resulting 10,000 particles are reduced to 5,000 particles after the update step. All filters represent the spatial pdf of each Bernoulli component by 1,000 particles. BP-LMB/P, BP-LMB, and BP-TOMB/P use 20 BP iterations to calculate the approximate marginal probabilities. The Gibbs sampler in Gibbs-LMB uses 100 samples for TS1 and 1,000 samples for TS2. All filters declare an object as detected if the existence probability of the corresponding Bernoulli component exceeds $\gamma_{\mathrm{D}} = 0.5$, and when this is

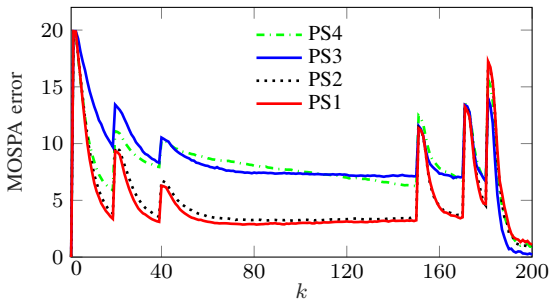

Fig. 5: MOSPA error of BP-LMB/P versus time for TS1 using parameter settings PS1 through PS4.

	γ_{tr}	γ_{C}	γ_{leg}
PS1	10^{-2}	10^{-10}	10^{-2}
PS2	10^{-2}	10^{-10}	10^{-1}
PS3	10^{-2}	10^{-3}	10^{-2}
PS4	10^{-1}	10^{-10}	10^{-2}

TABLE II: Threshold parameter settings (PSs) used for TS1.

the case, they calculate a sample mean approximation of (54) from the particle representation of the corresponding spatial pdf.

The birth statistics of all filters are established using the previous measurements $\boldsymbol{z}_{k-1}^{(m)}$, $m \in \mathcal{M}_{k-1}$. More precisely, BP-LMB/P and BP-TOMB/P choose their birth pdf as a mixture of the pdfs

$$\tilde{f}_{\text{B}}^{(m)}(\boldsymbol{x}_k) \propto \int f(\boldsymbol{x}_k|\boldsymbol{x}_{k-1}) f\big(\boldsymbol{z}_{k-1}^{(m)}\big|x_{1,k-1}, x_{2,k-1}\big) \times f_{\text{v}}(\dot{x}_{1,k-1}, \dot{x}_{2,k-1}) \mathrm{d}\boldsymbol{x}_{k-1},$$

for $m \in \mathcal{M}_{k-1}$. Here, $f\big(\boldsymbol{z}_{k-1}^{(m)}\big|x_{1,k-1}, x_{2,k-1}\big)$ is the likelihood function corresponding to our measurement model and $f_{\text{v}}(\dot{x}_{1,k-1}, \dot{x}_{2,k-1})$ is the pdf of independent, zero-mean, Gaussian random variables $\dot{x}_{1,k-1}$, $\dot{x}_{2,k-1}$ with variance 0.25. BP-LMB and Gibbs-LMB create a new Bernoulli component for each measurement $\boldsymbol{z}_{k-1}^{(m)}$, $m \in \mathcal{M}_{k-1}$, with spatial pdf $s_{\text{B}}^{(l=(k,m))}(\boldsymbol{x}_k) = \tilde{f}_{\text{B}}^{(m)}(\boldsymbol{x}_k)$. The mean number of newborn objects is $\mu_{\text{B}} = 0.1$ for all filters. In BP-LMB/P and BP-TOMB/P, the mean number of, respectively, unlabeled objects and undetected objects is initialized as 0.01.

B. Simulation Results

In Fig. 5, we study the performance of BP-LMB/P for TS1, using four different choices of the thresholds γ_{tr}, γ_{C}, and γ_{leg}. The figure displays the Euclidean distance based mean optimal subpattern assignment (MOSPA) metric with cutoff parameter $c = 20$ and order $p = 2$ [30] versus time k. Each curve is based on a specific threshold parameter setting (PS) and was obtained by averaging over 1,000 Monte Carlo runs. The PSs are defined by the values of γ_{tr}, γ_{C}, and γ_{leg} specified in Table II; in particular, PS2 uses a higher value of γ_{leg}, PS3 a higher value of γ_{C}, and PS4 a higher value of γ_{tr}.

One can see in Fig. 5 that the lowest MOSPA curve is achieved for PS1, i.e., for the lowest threshold values. However, a further reduction of the thresholds would not decrease the MOSPA curves further but would result in a higher filter runtime. If γ_{leg} is increased (as in PS2), then according to Section VII-A, there tend to be more Bernoulli components l such that $r_k^{(l)}$ falls below γ_{leg}, and which are hence transferred from the LMB part to the Poisson part. In challenging scenarios, such as low $p_{\text{D}}(\boldsymbol{x}_k)$ and/or high clutter, it is then possible that Bernoulli components are transferred to the Poisson part even though the corresponding objects exist, and this will generally reduce the tracking performance. If γ_{C} is increased (as in PS3), then according to Section VI-A and Appendix A, this generally results in a larger number of subsets $\mathbb{L}_{k-1}^{(c)}$, which may imply that some labeled objects are no longer correctly associated with the measurements and thus the tracking performance is again reduced. Finally, if γ_{tr} is increased (as in PS4), then according to Appendices B.2 and B.3, fewer Bernoulli components are transferred to the labeled RFS part, which may again result in a poorer tracking performance.

	γ_{tr}	γ_{C}	γ_{leg}	γ_{P}	γ_{T}
TS1	10^{-2}	10^{-10}	10^{-2}	10^{-3}	10^{-3}
TS2	10^{-3}	10^{-10}	10^{-3}	10^{-4}	10^{-4}

TABLE III: Thresholds γ_{tr}, γ_{C}, and γ_{leg} used by BP-LMB/P, γ_{P} used by BP-LMB and Gibbs-LMB, and γ_{T} used by BP-TOMB/P.

Therefore, for TS1, we will hereafter use the thresholds of PS1. These thresholds are shown again in Table III, along with the thresholds used in TS2. In fact, for the more challenging TS2, we observed that the thresholds in Table III resulted in a better MOSPA performance; in particular, we use smaller values of γ_{tr} and γ_{leg}. Table III furthermore shows the threshold γ_{P} used by BP-LMB and Gibbs-LMB for pruning Bernoulli components and the threshold γ_{T} used by BP-TOMB/P for transferring Bernoulli components of the MB part of the posterior state RFS to the Poisson part.

Fig. 4 shows an example of the estimated object trajectories obtained with BP-LMB/P for TS1 and for TS2, along with the true trajectories. One can see that the estimated trajectories closely match the true trajectories in both scenarios.

Fig. 6 compares the MOSPA performance of BP-LMB/P, Gibbs-LMB, BP-LMB, and BP-TOMB/P for TS1 and TS2. It is seen that for TS1, the performance of BP-LMB/P is almost identical to that of BP-LMB and BP-TOMB/P whereas the performance of Gibbs-LMB is noticeably poorer. For TS2, the results are similar except that the performance gap of Gibbs-LMB is much larger. This performance gap is due to the fact that Gibbs-LMB tends to ignore relevant association information in challenging scenarios. The amount of relevant association information taken into account by Gibbs-LMB grows with the number of samples used in the Gibbs sampler, but this comes at the cost of a higher computational complexity. In challenging scenarios such as TS2, more association information is required to obtain good results; this explains the larger performance gap of Gibbs-LMB in that case (even though for TS2, our Gibbs-LMB implementation used ten times more samples than for TS1). Overall, these results also demonstrate the excellent performance of the BP algorithm used by BP-LMB/P, BP-LMB, and BP-TOMB/P to compute the marginal association probabilities.

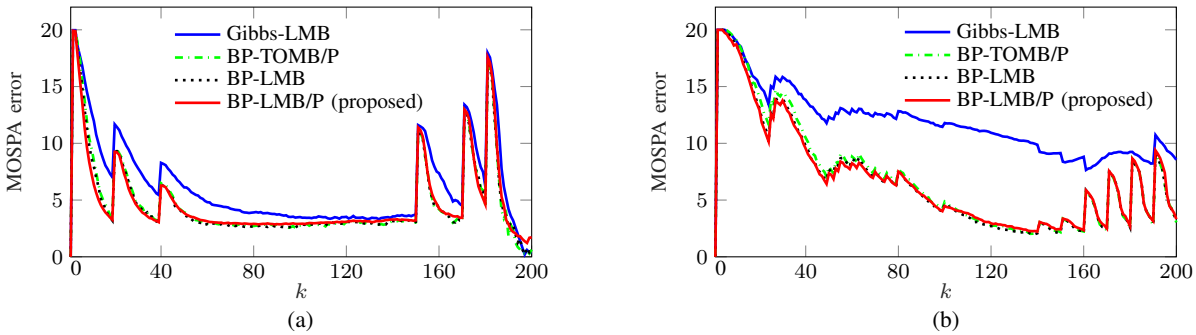

Fig. 6: MOSPA error of the four filters versus time for (a) TS1 and (b) TS2.

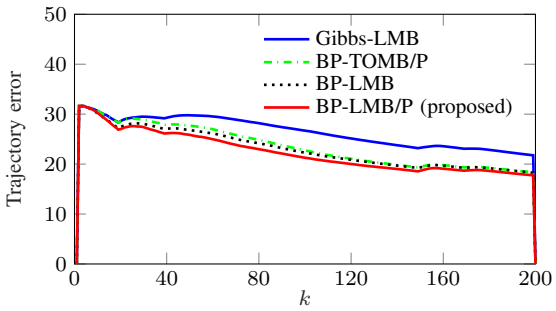

Fig. 7: Trajectory error of the four filters versus time for TS2.

In Fig. 7, we compare BP-LMB/P, Gibbs-LMB, BP-LMB, and BP-TOMB/P for TS2, using instead of the MOSPA metric the trajectory metric proposed in [31] with cutoff parameter $c = 20$, order $p = 2$, and switching penalty $\gamma = 2$. This metric can be decomposed into a "location error" (the location error of detected objects), a "false error" (caused by "false objects"), a "missed error" (caused by "missed objects"), and a "switching error." Here, false objects are detected objects that do not correspond to any object within the ground truth, whereas missed objects are objects within the ground truth that do not correspond to any detected object. Differently from the OSPA metric, the trajectory metric also takes into account the switching error caused by track switches, i.e., when a detected object is associated with different objects within the ground truth at different times. According to Fig. 7, the trajectory metric performance of BP-LMB/P is slightly better than that of BP-LMB and BP-TOMB/P and significantly better than that of Gibbs-LMB. These results agree with our MOSPA results in Fig. 6 (note the different y-axis scales used in the two figures). In addition, they show that BP-LMB/P also succeeds in estimating object trajectories, not just individual object states.

The four error components of the trajectory metric for TS2—i.e., location error, false error, missed error, and switching error—are shown individually in Fig. 8. Whereas for each error component the results of BP-LMB/P, BP-LMB, and BP-TOMB/P are quite similar, those of Gibbs-LMB are partly very different. This can be explained by the fact that Gibbs-LMB ignores valuable association information and thus detects some of the objects only with a delay or not at all. As a consequence, the number of missed objects is rather large, which leads to a significantly higher missed error (Fig. 8(c)). Furthermore, the smaller number of detected objects (compared to the other three filters) in turn implies a smaller number of false objects (Fig. 8(b)) and also lower location and switching errors (Figs. 8(a) and 8(d)).

It can also be seen that for all filters, the missed error shown in Fig. 8(c) is much higher than the other error components (note the widely different y-axis scale used in Fig. 8(c) compared to the other parts of Fig. 8). Thus, the missed error dominates the overall trajectory metric, which explains why Fig. 8(c) is similar to Fig. 7. Furthermore, the high missed error of Gibbs-LMB (compared to the other three filters) is not compensated by the fact that the other error components are lower. The other three filters, i.e., BP-LMB/P, BP-LMB, and BP-TOMB/P, exhibit a similar performance, with BP-LMB/P performing best. The latter fact can be attributed to the proposed transfer scheme between the Poisson part and the LMB part. Indeed, these simulation results suggest that our transfer scheme, with an appropriate choice of the thresholds γ_{tr}, γ_{leg}, and γ_{C}, can result in performance advantages compared to both BP-LMB (using a pruning of Bernoulli components) and BP-TOMB/P (using a recycling of Bernoulli components). These advantages come in addition to the lower filter runtimes obtained with BP-LMB/P, as reported presently.

Another trajectory metric that is closely related to the OSPA metric is the OSPA$^{(2)}$ metric proposed in [32]. In Fig. 9, we compare BP-LMB/P, Gibbs-LMB, BP-LMB, and BP-TOMB/P for TS2, using the OSPA$^{(2)}$ metric with cutoff parameter $c = 20$, order $p = 2$, and window length $L = 10$. The results are seen to be similar to those for the MOSPA error shown in Fig. 6(b). We note that for window length $L = 1$, the OSPA$^{(2)}$ metric would simplify to the OSPA metric.

Table IV lists the average runtime per time (k) step required by MATLAB implementations of the various filters on an Intel quad core i7-6600U CPU. Also shown is the average number of Bernoulli components per time step employed by each filter. Again, these numbers were obtained by averaging over 1,000 Monte Carlo runs. One can see that BP-LMB/P achieves the lowest runtimes of all filters; furthermore, it employs the lowest numbers of Bernoulli components of all filters except Gibbs-LMB. We note that, as is demonstrated by Fig. 6, this low complexity of BP-LMB/P does not come at the cost of a poorer MOSPA performance. Also, while Gibbs-LMB employs fewer Bernoulli components (especially for TS2), its MOSPA performance for TS2 is significantly poorer.

We can conclude from the results in Figs. 6–9 and Table IV that BP-LMB/P offers a superior performance-complexity

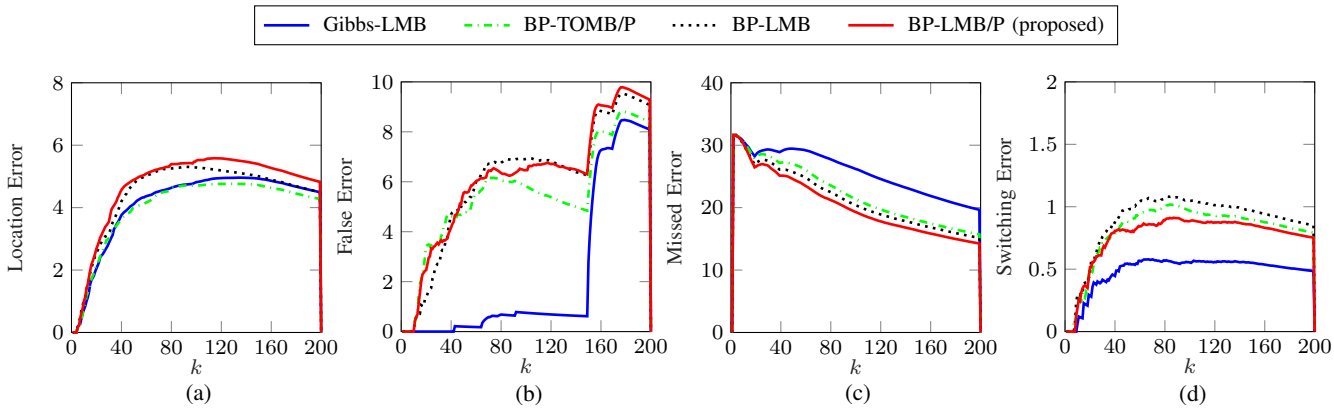

Fig. 8: Individual components of the trajectory metric of the four filters versus time for TS2: (a) location error, (b) false error, (c) missed error, and (d) switching error.

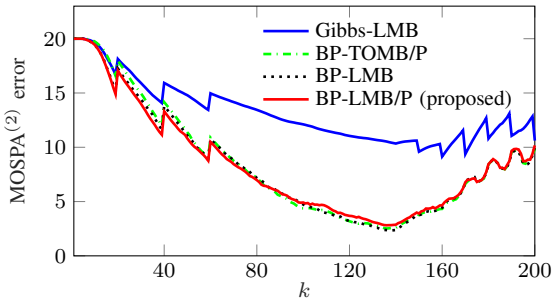

Fig. 9: MOSPA$^{(2)}$ error of the four filters versus time for TS2.

Filter	RT-TS1	RT-TS2	NBC-TS1	NBC-TS2
BP-LMB/P (proposed)	1.33 s	5.05 s	15.21	162.82
Gibbs-LMB	5.12 s	7.94 s	9.69	34.23
BP-LMB	5.55 s	21.68 s	34.15	861.96
BP-TOMB/P	10.66 s	16.09 s	63.33	521.93

TABLE IV: Measured complexity of the four filters for TS1 and TS2. RT-TS1 and RT-TS2 designate the average runtime per time step, and NBC-TS1 and NBC-TS2 designate the average number of Bernoulli components per time step.

compromise relative to the other filters. It has a significantly better performance than Gibbs-LMB (especially for TS2) and also a lower runtime. When compared to BP-LMB and BP-TOMB/P, the runtime of BP-LMB/P is much lower while its performance is almost identical. The low runtime of BP-LMB/P is a direct consequence of the fact that objects of unlikely existence are modeled by the Poisson RFS. The performance advantage of BP-LMB/P over Gibbs-LMB is mainly due to the fact that BP-LMB/P takes into account more association information. Gibbs-LMB ignores relevant association information, which allows it to employ fewer Bernoulli components but also results in a poorer performance. For challenging scenarios with a high number of (closely spaced) objects and/or a low detection probability and/or strong clutter, the number of samples used by the Gibbs sampler must be increased significantly to obtain an acceptable MOSPA performance, and this entails a higher complexity.

X. Conclusion

We proposed an efficient multiobject tracking algorithm that maintains track continuity. Low complexity is achieved by a combination of a labeled multi-Bernoulli random finite set (RFS) and a Poisson RFS as well as complexity-reducing approximations in the update step. Objects of unlikely existence are tracked in an efficient manner by the Poisson RFS, and a new labeled Bernoulli component is created and maintained only if the existence of an object is sufficiently likely. Our simulation results showed that the proposed algorithm offers an attractive accuracy-complexity compromise. The complexity is significantly smaller than that of other RFS-based algorithms with comparable performance, especially in scenarios with many objects and strong clutter. Interesting directions of future research include extensions of our algorithm to multiple-detection measurement models and multi-sensor scenarios [19], [33]–[36].

Appendix A

In Table V, we present an algorithm for constructing the partitionings (32) and (33). This algorithm is further explained in the following. In Step 1, the sets $\mathcal{M}_k(l) \subseteq \mathcal{M}_k$ comprise the indices of all those measurements whose association with the object with state $(\mathbf{x}_k, l)$ is plausible. (Note that the $\mathcal{M}_k(l)$ for different $l \in \mathbb{L}_{k-1}^*$ are not necessarily disjoint.) Then, after an initialization step in Step 2, we perform the iterative procedure constituted by Step 3, which generates the label subsets $\mathbb{L}_{k-1}^{(c)} \subseteq \mathbb{L}_{k-1}^*$, $c \in \{1, \ldots, C\}$ and the corresponding measurement index subsets $\mathcal{M}_k^{(c)} \subseteq \mathcal{M}_k$, $c \in \{1, \ldots, C\}$.

The generation of these subsets is done such that for each $c \in \{1, \ldots, C\}$, the association of an object state $(\mathbf{x}_k, l)$, $l \in \mathbb{L}_{k-1}^{(c)}$ with a measurement index m is plausible for $m \in \mathcal{M}_k^{(c)}$ and implausible for $m \in \mathcal{M}_k^{(c')}$ with $c' \neq c$. This is achieved by doing the following for each $l^{(j)} \in \mathbb{L}_{k-1}^*$: In Step 3.1, we determine the subset $\mathcal{C}'$ of those indices $c \in \{1, \ldots, C\}$ for which the measurement index subsets $\mathcal{M}_k^{(c)} \subseteq \mathcal{M}_k$ have some elements in common with $\mathcal{M}_k(l^{(j)})$, i.e., with the measurement indices corresponding to object state $(\mathbf{x}_k, l^{(j)})$; this expresses the fact that the association between object state $(\mathbf{x}_k, l^{(j)})$ and some measurement indices from $\bigcup_{c' \in \mathcal{C}'} \mathcal{M}_k^{(c')}$ is plausible. If none of the $\mathcal{M}_k^{(c)}$ has an element in common with

TABLE V: Algorithm for constructing the partitionings (32) and (33)

Input: Label set $\mathbb{L}^*_{k-1} = \{l^{(1)}, \ldots, l^{(|\mathbb{L}^*_{k-1}|)}\}$; measurement index set $\mathcal{M}_k$; association weight $\beta_k^{(l,m)}$; threshold γ_{C}.

Output: Number of subsets C, label subsets $\mathbb{L}^{(c)}_{k-1}$, $c \in \{1, \ldots, C\}$; measurement index subsets $\mathcal{M}^{(c)}_k$, $c \in \{1, \ldots, C\}$ and $\mathcal{M}^{\text{res}}_k$.

Operations:

1) For each $l \in \mathbb{L}^*_{k-1}$, determine $\mathcal{M}_k(l) \subseteq \mathcal{M}_k$ as the subset of all measurement indices $m \in \mathcal{M}_k$ for which $\beta_k^{(l,m)} \geq \gamma_{\mathrm{C}}$.
2) Initialization: Set $C = 1$, $\mathbb{L}^{(1)}_{k-1} = \{l^{(1)}\}$, and $\mathcal{M}^{(1)}_k = \mathcal{M}_k(l^{(1)})$.
3) Iteration: For $j = 2, \ldots, |\mathbb{L}^*_{k-1}|$, do the following:
   3.1) Determine $\mathcal{C}' \subseteq \{1, \ldots, C\}$ as the set of all $c \in \{1, \ldots, C\}$ for which $\mathcal{M}^{(c)}_k \cap \mathcal{M}_k(l^{(j)}) \neq \emptyset$.
   3.2) If $\mathcal{C}' = \emptyset$, then increment C by one and set $\mathbb{L}^{(C)}_{k-1} = \{l^{(j)}\}$ and $\mathcal{M}^{(C)}_k = \mathcal{M}_k(l^{(j)})$; else do the following:
   - Select an arbitrary $c \in \mathcal{C}'$ and set $\mathbb{L}^{(c)}_{k-1} = \{l^{(j)}\} \cup \bigcup_{c' \in \mathcal{C}'} \mathbb{L}^{(c')}_{k-1}$ and $\mathcal{M}^{(c)}_k = \mathcal{M}_k(l^{(j)}) \cup \bigcup_{c' \in \mathcal{C}'} \mathcal{M}^{(c')}_k$.
   - Set $\mathcal{C}'' = (\{1, \ldots, C\} \setminus \mathcal{C}') \cup \{c\}$ and $C = |\mathcal{C}''|$.
   - Perform a reindexing whereby the indices contained in $\mathcal{C}''$ are replaced by the new indices $1, 2, \ldots, C$.
4) Set $\mathcal{M}^{\text{res}}_k = \mathcal{M}_k \setminus \bigcup_{c \in \{1,\ldots,C\}} \mathcal{M}^{(c)}_k$.

$\mathcal{M}_k(l^{(j)})$, i.e., if the association between object state $(\mathbf{x}_k, l^{(j)})$ with *any* measurement index $m \in \bigcup_{c \in \{1,\ldots,C\}} \mathcal{M}^{(c)}_k$ is implausible, then $\mathcal{C}'$ is empty. In that case, C is incremented by 1, and a new label subset and a new measurement index subset are created as $\mathbb{L}^{(C)}_{k-1} = \{l^{(j)}\}$ and $\mathcal{M}^{(C)}_k = \mathcal{M}_k(l^{(j)})$, respectively (see Step 3.2). Otherwise, i.e., if $|\mathcal{C}'| \geq 1$, we merge all the label subsets $\mathbb{L}^{(c')}_{k-1}$ with $c' \in \mathcal{C}'$ as well as the considered label $l^{(j)}$ into one common label subset $\mathbb{L}^{(c)}_{k-1}$, and we merge all the corresponding measurement index subsets $\mathcal{M}^{(c')}_k$, $c' \in \mathcal{C}'$ as well as $\mathcal{M}_k(l^{(j)})$ into one common measurement index subset $\mathcal{M}^{(c)}_k$ (see Step 3.2, first bullet item). Here, the index c is picked arbitrarily from $\mathcal{C}'$. Next, we perform a reindexing such that the index values in $\mathcal{C}'' \triangleq (\{1, \ldots, C\} \setminus \mathcal{C}') \cup \{c\}$ become $1, 2, \ldots, |\mathcal{C}''|$. Furthermore, we update C as $C = |\mathcal{C}''|$, so that the new set of subset indices is given by $\{1, \ldots, C\}$ (see Step 3.2, second and third bullet items). Subsequently, Steps 3.1 and 3.2 are repeated for the next $l^{(j)} \in \mathbb{L}^*_{k-1}$ (if available).

The final number C of subsets $\mathbb{L}^{(c)}_{k-1}$, $c \in \{1, \ldots, C\}$ is determined by this iterative procedure. Finally, in Step 4, the measurement indices $m \in \mathcal{M}_k$ that are not part of any subset $\mathcal{M}^{(c)}_k$ are collected in $\mathcal{M}^{\text{res}}_k$. We note that a larger threshold γ_{C} used in the definition of the sets $\mathcal{M}_k(l)$ in Step 1 tends to result in smaller subsets $\mathcal{M}_k(l)$, $\mathbb{L}^{(c)}_{k-1}$, and $\mathcal{M}^{(c)}_k$, a larger residual set $\mathcal{M}^{\text{res}}_k$, a larger number C of subsets $\mathbb{L}^{(c)}_{k-1}$ and $\mathcal{M}^{(c)}_k$, and a higher probability of $\mathcal{C}'$ being empty.

APPENDIX B

We will derive the approximation of the posterior pgfl $G_{\tilde{\mathsf{X}}_k, \mathsf{X}_k}[\tilde{h}, h | Z_{1:k}]$ given by (34) and subsequent equations.

B.1 Pruning and Clustering

Our approximation is based on the partitioning of the label set $\mathbb{L}^{(*)}_{k-1}$ in (32) and the partitioning of the measurement index set $\mathcal{M}_k$ in (33). As described in Section VI-A, only the associations between objects with labeled state $(\mathbf{x}_k, l)$, $l \in \mathbb{L}^{(c)}_{k-1}$ and measurements with index $m \in \mathcal{M}^{(c)}_k$ are plausible. Thus, by pruning all the association hypotheses $\boldsymbol{a}_k \in \mathcal{A}_k$ that associate some $l \in \mathbb{L}^{(c)}_{k-1}$ with some $m \in \mathcal{M}_k \setminus \mathcal{M}^{(c)}_k$, we obtain a more efficient representation of the *relevant* association information. Let $\mathcal{A}^{\text{rem}}_k \subseteq \mathcal{A}_k$ denote the set of the remaining (nonpruned) $\boldsymbol{a}_k$. Note that our pruning does not include missed detections (described by $a^{(l)}_k = 0$), i.e., all $\boldsymbol{a}_k$ with $a^{(l)}_k = 0$, $l \in \mathbb{L}^{(c)}_{k-1}$ are part of $\mathcal{A}^{\text{rem}}_k$. Therefore, each $\boldsymbol{a}_k \in \mathcal{A}^{\text{rem}}_k$ associates each object label $l \in \mathbb{L}^{(c)}_{k-1}$ with some measurement index $m \in \{0\} \cup \mathcal{M}^{(c)}_k$. (Note, also, that an $\boldsymbol{a}_k \in \mathcal{A}^{\text{rem}}_k$ does not associate any object label with any $m \in \mathcal{M}^{\text{res}}_k$.)

The pruning yields the following approximation of $G'_{\tilde{\mathsf{X}}_k, \mathsf{X}_k}[\tilde{h}, h]$ in (18):

$$G'_{\tilde{\mathsf{X}}_k, \mathsf{X}_k}[\tilde{h}, h] \approx \sum_{\boldsymbol{a}_k \in \mathcal{A}^{\text{rem}}_k} w_{\boldsymbol{a}_k} L_{\mathbb{L}^*_{k-1}}\big[\tilde{h}; r_k^{(\cdot, a_k^{(\cdot)})}, s_k^{(\cdot, a_k^{(\cdot)})}\big] \times M_{\mathcal{M}_{\boldsymbol{a}_k}}\big[h; \bar{r}_k^{(\cdot)}, \bar{s}_k^{(\cdot)}\big]. \quad (55)$$

Using the fact that the Bernoulli component factors in $M_{\mathcal{M}_{\boldsymbol{a}_k}}\big[h; \bar{r}_k^{(\cdot)}, \bar{s}_k^{(\cdot)}\big]$ with $m \in \mathcal{M}^{\text{res}}_k \subseteq \mathcal{M}_{\boldsymbol{a}_k}$ appear in each one of the summation terms in (55), we obtain further

$$G'_{\tilde{\mathsf{X}}_k, \mathsf{X}_k}[\tilde{h}, h] \approx M_{\mathcal{M}^{\text{res}}_k}\big[h; \bar{r}_k^{(\cdot)}, \bar{s}_k^{(\cdot)}\big] \sum_{\boldsymbol{a}_k \in \mathcal{A}^{\text{rem}}_k} w_{\boldsymbol{a}_k} L_{\mathbb{L}^*_{k-1}}\big[\tilde{h}; r_k^{(\cdot, a_k^{(\cdot)})}, s_k^{(\cdot, a_k^{(\cdot)})}\big] \times M_{\mathcal{M}_{\boldsymbol{a}_k} \setminus \mathcal{M}^{\text{res}}_k}\big[h; \bar{r}_k^{(\cdot)}, \bar{s}_k^{(\cdot)}\big]. \quad (56)$$

Here, the $w_{\boldsymbol{a}_k}$ are given by expression (20).

As a consequence of the pruning, all objects with labels $l \in \mathbb{L}^{(c)}_{k-1}$, i.e., corresponding to cluster c, are now associated only with measurements of the same cluster c, $m \in \{0\} \cup \mathcal{M}^{(c)}_k$, and not with any other measurements $m \in \mathcal{M}_k \setminus \mathcal{M}^{(c)}_k$. This implies that each entry $a^{(l)}_k$ of $\boldsymbol{a}_k \in \mathcal{A}^{\text{rem}}_k$ associates labels $l \in \mathbb{L}^{(c)}_{k-1}$ of cluster c only with measurements $m \in \{0\} \cup \mathcal{M}^{(c)}_k$ of cluster c. Therefore, a_k (of dimension $|\mathbb{L}^*_{k-1}|$) can be split into C subvectors $\mathsf{a}'^{(c)}_k \in \big(\{0\} \cup \mathcal{M}^{(c)}_k\big)^{|\mathbb{L}^{(c)}_{k-1}|}$, $c \in \mathcal{C}$ of lower dimensions $|\mathbb{L}^{(c)}_{k-1}|$. Here, the entry $\mathsf{a}'^{(c,l)}_k$ of $\mathsf{a}'^{(c)}_k$, with $l \in \mathbb{L}^{(c)}_{k-1}$, is defined similarly to $\mathsf{a}^{(l)}_k$ in Section V-A as $\mathsf{a}'^{(c,l)}_k \triangleq m \in \mathcal{M}^{(c)}_k$ if the labeled object with state $(\mathbf{x}_k, l)$ generates measurement $\boldsymbol{z}^{(m)}_k$ and $\mathsf{a}'^{(c,l)}_k \triangleq 0$ if it does not generate a measurement. The admissible association vectors $\boldsymbol{a}'^{(c)}_k$ (where admissibility was defined in Section V-A) are collected in the association alphabet $\mathcal{A}'^{(c)}_k$. We can now factor the weights as

$$w_{\boldsymbol{a}_k} = \prod_{c \in \mathcal{C}} w_{\boldsymbol{a}'^{(c)}_k}, \quad (57)$$

where (cf. (20))

$$w_{\boldsymbol{a}'^{(c)}_k} \propto \left(\prod_{l \in \mathbb{L}^{(c)}_{k-1}} \beta_k^{(l, a'^{(c,l)}_k)} \right) \prod_{m \in \mathcal{M}_{\boldsymbol{a}'^{(c)}_k}} \beta_k^{(m)}.$$

Here, $\mathcal{M}_{\boldsymbol{a}_k'^{(c)}} \subseteq \mathcal{M}_k^{(c)}$ comprises all measurement indices $m \in \mathcal{M}_k^{(c)}$ that are not associated with any labeled object via $\boldsymbol{a}_k'^{(c)} \in \mathcal{A}_k'^{(c)}$ and, thus, originate from an unlabeled object or from clutter. In particular, $\mathcal{M}_{\boldsymbol{a}_k'^{(c)}} = \emptyset$ indicates that all $m \in \mathcal{M}_k^{(c)}$ are associated with an object with label $l \in \mathbb{L}_{k-1}^{(c)}$. Furthermore, we have

$$L_{\mathbb{L}_{k-1}^*}\big[\tilde{h}; r_k^{(\cdot,a_k^{(\cdot)})}, s_k^{(\cdot,a_k^{(\cdot)})}\big] = \prod_{c\in\mathcal{C}} L_{\mathbb{L}_{k-1}^{(c)}}\big[\tilde{h}; r_k^{(\cdot,a_k'^{(c,\cdot)})}, s_k^{(\cdot,a_k'^{(c,\cdot)})}\big], \tag{58}$$

$$M_{\mathcal{M}_{\boldsymbol{a}_k}\setminus\mathcal{M}_k^{\text{res}}}\big[h; \bar{r}_k^{(\cdot)}, \bar{s}_k^{(\cdot)}\big] = \prod_{c\in\mathcal{C}} M_{\mathcal{M}_{\boldsymbol{a}_k'^{(c)}}}\big[h; \bar{r}_k^{(\cdot)}, \bar{s}_k^{(\cdot)}\big]. \tag{59}$$

Using the factorizations (57)–(59) as well as the identity $\sum_{\boldsymbol{a}_k\in\mathcal{A}_k^{\text{rem}}} = \sum_{\boldsymbol{a}_k'^{(1)}\in\mathcal{A}_k'^{(1)}} \cdots \sum_{\boldsymbol{a}_k'^{(C)}\in\mathcal{A}_k'^{(C)}}$, we can rewrite the approximation (56) in terms of the $\boldsymbol{a}_k'^{(c)}$ as

$$G'_{\tilde{\mathsf{X}}_k,\mathsf{X}_k}[\tilde{h},h] \approx M_{\mathcal{M}_k^{\text{res}}}\big[h; \bar{r}_k^{(\cdot)}, \bar{s}_k^{(\cdot)}\big] \prod_{c\in\mathcal{C}} G^{(c)}[\tilde{h},h], \tag{60}$$

where

$$G^{(c)}[\tilde{h},h] \triangleq \sum_{\boldsymbol{a}_k'^{(c)}\in\mathcal{A}_k'^{(c)}} w_{\boldsymbol{a}_k'^{(c)}} L_{\mathbb{L}_{k-1}^{(c)}}\big[\tilde{h}; r_k^{(\cdot,a_k'^{(c,\cdot)})}, s_k^{(\cdot,a_k'^{(c,\cdot)})}\big] \times M_{\mathcal{M}_{\boldsymbol{a}_k'^{(c)}}}\big[h; \bar{r}_k^{(\cdot)}, \bar{s}_k^{(\cdot)}\big]. \tag{61}$$

We note that $G^{(c)}[\tilde{h},h]$ and $M_{\mathcal{M}_k^{\text{res}}}\big[h; \bar{r}_k^{(\cdot)}, \bar{s}_k^{(\cdot)}\big]$ represent *clustered* objects and *nonclustered* objects, respectively, which, in both cases, may be likely or unlikely to exist.

So far, we approximated $G'_{\tilde{\mathsf{X}}_k,\mathsf{X}_k}[\tilde{h},h]$ in (18) by expression (60), which is the product of the C LMB–MB mixture pgfls $G^{(c)}[\tilde{h},h]$ in (61) and the MB pgfl $M_{\mathcal{M}_k^{\text{res}}}\big[h; \bar{r}_k^{(\cdot)}, \bar{s}_k^{(\cdot)}\big]$. As visualized in Fig. 3, this is the first step in a series of pgfl approximations or modifications that are used in the development of the proposed LMB/P filter. Next, we will develop approximations of $G^{(c)}[\tilde{h},h]$ and $M_{\mathcal{M}_k^{\text{res}}}\big[h; \bar{r}_k^{(\cdot)}, \bar{s}_k^{(\cdot)}\big]$.

B.2 Approximation of the pgfl of Clustered Objects

We will approximate the pgfl representing clustered objects, $G^{(c)}[\tilde{h},h]$, by an LMBM pgfl. To this end, we recall from Section B.1 that the MB pgfl $M_{\mathcal{M}_{\boldsymbol{a}_k'^{(c)}}}\big[h; \bar{r}_k^{(\cdot)}, \bar{s}_k^{(\cdot)}\big]$ involved in $G^{(c)}[\tilde{h},h]$ in (61) corresponds to measurements $m \in \mathcal{M}_k^{(c)}$ that originate from an unlabeled object or from clutter. We want to transfer unlabeled objects that are likely to exist, or, more specifically, (unlabeled) Bernoulli components $B\big[h; \bar{r}_k^{(m)}, \bar{s}_k^{(m)}\big]$, $m \in \mathcal{M}_{\boldsymbol{a}_k'^{(c)}}$ with $\bar{r}_k^{(m)} \geq \gamma_{\text{tr}}$, to the labeled RFS part. Here, $\bar{r}_k^{(m)}$ is given by (28). This transfer is motivated by the fact that the labeled RFS part guarantees track continuity and, after further modifications that are described in Section VII, achieves a higher tracking accuracy than the unlabeled RFS part. The transfer is accomplished by formally replacing the measurement index m arising in $B\big[h; \bar{r}_k^{(m)}, \bar{s}_k^{(m)}\big]$ by the label $l = (k,m)$. Let $\mathbb{L}_k^{(c)\text{tr}}$ collect the labels of the transferred Bernoulli components, i.e., all $l = (k,m)$ with $m \in \mathcal{M}_k^{(c)}$ such that $\bar{r}^{(m)} \geq \gamma_{\text{tr}}$ (see also Fig. 1). We note that a higher threshold γ_{tr} tends to imply a smaller number of transferred Bernoulli components, $|\mathbb{L}_k^{(c)\text{tr}}|$. Furthermore, since the other Bernoulli components $B\big[h; \bar{r}_k^{(m)}, \bar{s}_k^{(m)}\big]$ (with $\bar{r}_k^{(m)} < \gamma_{\text{tr}}$) are unlikely, we prune them. This is done by setting $h = 1$ because $B\big[1; \bar{r}_k^{(m)}, \bar{s}_k^{(m)}\big] = 1$.

With these modifications, and by introducing the association vector $\mathbf{a}_k^{(c)}$ as in Section VI-B, $G^{(c)}[\tilde{h},h]$ in (61) is replaced by $G^{(c)}[\tilde{h}]$ as defined in (36) (see Fig. 3). Accordingly, Eq. (60) becomes

$$G'_{\tilde{\mathsf{X}}_k,\mathsf{X}_k}[\tilde{h},h] \approx M_{\mathcal{M}_k^{\text{res}}}\big[h; \bar{r}_k^{(\cdot)}, \bar{s}_k^{(\cdot)}\big] \prod_{c\in\mathcal{C}} G^{(c)}[\tilde{h}]. \tag{62}$$

B.3 Approximation of the pgfl of Nonclustered Objects

Next, we consider $M_{\mathcal{M}_k^{\text{res}}}\big[h; \bar{r}_k^{(\cdot)}, \bar{s}_k^{(\cdot)}\big]$ in (62). Similarly to the measurements $m \in \mathcal{M}_{\boldsymbol{a}_k'^{(c)}}$ involved in $M_{\mathcal{M}_{\boldsymbol{a}_k'^{(c)}}}\big[h; \bar{r}_k^{(\cdot)}, \bar{s}_k^{(\cdot)}\big]$ in (61), the measurements $m \in \mathcal{M}_k^{\text{res}}$ involved in $M_{\mathcal{M}_k^{\text{res}}}\big[h; \bar{r}_k^{(\cdot)}, \bar{s}_k^{(\cdot)}\big]$ originate from an unlabeled object or from clutter. As in Section B.2, we transfer objects that are likely to exist to the labeled RFS part, and thus we formally replace the measurement index m in each Bernoulli component $B\big[h; \bar{r}_k^{(m)}, \bar{s}_k^{(m)}\big]$, $m \in \mathcal{M}_k^{\text{res}}$ of $M_{\mathcal{M}_k^{\text{res}}}\big[h; \bar{r}_k^{(\cdot)}, \bar{s}_k^{(\cdot)}\big]$ with $\bar{r}_k^{(m)} \geq \gamma_{\text{tr}}$ by the label $l = (k,m)$. These labels are collected in $\mathbb{L}_k^{\text{res,tr}}$ (see Fig. 1), and the corresponding measurement indices are collected in $\mathcal{M}_k^{\text{res,tr}} \subseteq \mathcal{M}_k^{\text{res}}$ (see Fig. 2). The remaining measurement indices are collected in $\mathcal{M}_k' = \mathcal{M}_k^{\text{res}} \setminus \mathcal{M}_k^{\text{res,tr}}$ (again see Fig. 2). As before, a higher threshold γ_{tr} tends to imply a smaller number of transferred Bernoulli components, $|\mathbb{L}_k^{\text{res,tr}}|$.

Using these modifications, $M_{\mathcal{M}_k^{\text{res}}}\big[h; \bar{r}_k^{(\cdot)}, \bar{s}_k^{(\cdot)}\big]$ is approximated according to (see Fig. 3)

$$M_{\mathcal{M}_k^{\text{res}}}\big[h; \bar{r}_k^{(\cdot)}, \bar{s}_k^{(\cdot)}\big] \approx L_{\mathbb{L}_k'^{\text{res,tr}}}\big[\tilde{h}; \bar{r}_k^{(\cdot)}, \bar{s}_k^{(\cdot)}\big] M_{\mathcal{M}_k'}\big[h; \bar{r}_k^{(\cdot)}, \bar{s}_k^{(\cdot)}\big]. \tag{63}$$

Inserting (63) into (62) yields $G'_{\tilde{\mathsf{X}}_k,\mathsf{X}_k}[\tilde{h},h] \approx L_{\mathbb{L}_k'^{\text{res,tr}}}\big[\tilde{h}; \bar{r}_k^{(\cdot)}, \bar{s}_k^{(\cdot)}\big] \times M_{\mathcal{M}_k'}\big[h; \bar{r}_k^{(\cdot)}, \bar{s}_k^{(\cdot)}\big] \prod_{c\in\mathcal{C}} G^{(c)}[\tilde{h}]$. Finally, inserting this latter approximation into (17) and grouping terms, we obtain (34), (35), and (39) (again see Fig. 3).

REFERENCES

[1] Y. Bar-Shalom, P. K. Willett, and X. Tian, *Tracking and Data Fusion: A Handbook of Algorithms*. Storrs, CT, USA: Yaakov Bar-Shalom, 2011.

[2] R. P. S. Mahler, *Statistical Multisource-Multitarget Information Fusion*. Boston, MA, USA: Artech House, 2007.

[3] ——, *Advances in Statistical Multisource-Multitarget Information Fusion*. Boston, MA, USA: Artech House, 2014.

[4] S. Challa, M. R. Morelande, D. Musicki, and R. Evans, *Fundamentals of Object Tracking*. Cambridge, UK: Cambridge University Press, 2011.

[5] S. Blackman and R. Popoli, *Design and Analysis of Modern Tracking Systems*. Norwood, MA, USA: Artech House, 1999.

[6] R. P. S. Mahler, "Multitarget Bayes filtering via first-order multitarget moments," *IEEE Trans. Aerosp. Electron. Syst.*, vol. 39, no. 4, pp. 1152–1178, Oct. 2003.

[7] ——, "PHD filters of higher order in target number," *IEEE Trans. Aerosp. Electron. Syst.*, vol. 43, no. 4, pp. 1523–1543, Oct. 2007.

[8] B.-T. Vo, B.-N. Vo, and A. Cantoni, "The cardinality balanced multi-target multi-Bernoulli filter and its implementations," *IEEE Trans. Signal Process.*, vol. 57, no. 2, pp. 409–423, Feb. 2009.

[9] B.-T. Vo and B.-N. Vo, "Labeled random finite sets and multi-object conjugate priors," *IEEE Trans. Signal Process.*, vol. 61, no. 13, pp. 3460–3475, Jul. 2013.

[10] B.-N. Vo, B.-T. Vo, and D. Phung, "Labeled random finite sets and the Bayes multi-target tracking filter," *IEEE Trans. Signal Process.*, vol. 62, no. 24, pp. 6554–6567, Dec. 2014.

[11] S. Reuter, B.-T. Vo, B.-N. Vo, and K. Dietmayer, "The labeled multi-Bernoulli filter," *IEEE Trans. Signal Process.*, vol. 62, no. 12, pp. 3246–3260, Jun. 2014.

[12] S. Reuter, A. Danzer, M. Stübler, A. Scheel, and K. Granström, "A fast implementation of the labeled multi-Bernoulli filter using Gibbs sampling," in *Proc. IVS-17*, Los Angeles, CA, USA, Jun. 2017, pp. 765–772.

[13] T. Kropfreiter, F. Meyer, and F. Hlawatsch, "A fast labeled multi-Bernoulli filter using belief propagation," *IEEE Trans. Aerosp. Electron. Syst.*, vol. 56, no. 3, pp. 2478–2488, Jun. 2020.

[14] B.-N. Vo, B.-T. Vo, and H. G. Hoang, "An efficient implementation of the generalized labeled multi-Bernoulli filter," *IEEE Trans. Signal Process.*, vol. 65, no. 8, pp. 1975–1987, 2017.

[15] M. Beard, B.-T. Vo, and B.-N. Vo, "A solution for large-scale multi-object tracking," *IEEE Trans. Signal Process.*, vol. 68, pp. 2754–2769, 2020.

[16] B.-N. Vo and B.-T. Vo, "A multi-scan labeled random finite set model for multi-object state estimation," *IEEE Trans. Signal Process.*, vol. 67, no. 19, pp. 4948–4963, 2019.

[17] J. L. Williams, "Marginal multi-Bernoulli filters: RFS derivation of MHT, JIPDA, and association-based MeMBer," *IEEE Trans. Aerosp. Electron. Syst.*, vol. 51, no. 3, pp. 1664–1687, Jul. 2015.

[18] ——, "Hybrid Poisson and multi-Bernoulli filters," in *Proc. FUSION-12*, Singapore, Jul. 2012, pp. 1103–1110.

[19] F. Meyer, T. Kropfreiter, J. L. Williams, R. A. Lau, F. Hlawatsch, P. Braca, and M. Z. Win, "Message passing algorithms for scalable multitarget tracking," *Proc. IEEE*, vol. 106, no. 2, pp. 221–259, Feb. 2018.

[20] J. Houssineau and D. E. Clark, "Multitarget filtering with linearized complexity," *IEEE Trans. Signal Process.*, vol. 66, no. 18, pp. 4957–4970, 2018.

[21] Á. F. García-Fernández, L. Svensson, and M. R. Morelande, "Multiple target tracking based on sets of trajectories," *IEEE Trans. Aerosp. Electron. Syst.*, vol. 56, no. 3, pp. 1685–1707, Jun. 2020.

[22] K. Granström, L. Svensson, Y. Xia, J. Williams, and Á. F. García-Fernández, "Poisson multi-Bernoulli mixture trackers: Continuity through random finite sets of trajectories," in *Proc. FUSION-18*, Cambridge, UK, Jul. 2018, pp. 973–981.

[23] Á. F. García-Fernández and L. Svensson, "Trajectory PHD and CPHD filters," *IEEE Trans. Signal Process.*, vol. 67, no. 22, pp. 5702–5714, Nov. 2019.

[24] Y. Xia, K. Granström, L. Svensson, Á. F. García-Fernández, and J. L. Williams, "Multiscan implementation of the trajectory Poisson multi-Bernouli mixture filter," *J. Adv. Inf. Fusion*, vol. 14, no. 2, pp. 213–235, Dec. 2019.

[25] T. Kropfreiter and F. Hlawatsch, "Multiobject tracking with track continuity: An efficient random finite set based algorithm," in *Proc. SDF-18*, Bonn, Germany, Oct. 2018.

[26] Á. F. García-Fernández and B.-N. Vo, "Derivation of the PHD and CPHD filters based on direct Kullback-Leibler divergence minimization," *IEEE Trans. Signal Process.*, vol. 63, no. 21, pp. 5812–5820, Nov. 2015.

[27] F. Meyer, P. Braca, P. Willett, and F. Hlawatsch, "A scalable algorithm for tracking an unknown number of targets using multiple sensors," *IEEE Trans. Signal Process.*, vol. 65, no. 13, pp. 3478–3493, Jul. 2017.

[28] Y. Bar-Shalom, X.-R. Li, and T. Kirubarajan, *Estimation with Applications to Tracking and Navigation*. New York, NY, USA: Wiley, 2002.

[29] T. Kropfreiter, F. Meyer, and F. Hlawatsch, "Sequential Monte Carlo implementation of the track-oriented marginal multi-Bernoulli/Poisson filter," in *Proc. FUSION-16*, Heidelberg, Germany, Jul. 2016, pp. 972–979.

[30] D. Schuhmacher, B.-T. Vo, and B.-N. Vo, "A consistent metric for performance evaluation of multi-object filters," *IEEE Trans. Signal Process.*, vol. 56, no. 8, pp. 3447–3457, Aug. 2008.

[31] Á. F. García-Fernández, A. S. Rahmathullah, and L. Svensson, "A metric on the space of finite sets of trajectories for evaluation of multi-target tracking algorithms," *IEEE Trans. Signal Process.*, vol. 68, pp. 3917–3928, Jun. 2020.

[32] M. Beard, B.-T. Vo, and B.-N. Vo, "OSPA$^{(2)}$: Using the OSPA metric to evaluate multi-target tracking performance," in *Proc. ICCAIS-17*, Chiang Mai, Thailand, Oct. 2017, pp. 86–91.

[33] F. Meyer and J. L. Williams, "Scalable detection and tracking of geometric extended objects," *IEEE Trans. Signal Process.*, vol. 69, pp. 6283–6298, Oct. 2021.

[34] M. Beard, S. Reuter, K. Granström, B.-T. Vo, B.-N. Vo, and A. Scheel, "Multiple extended target tracking with labeled random finite sets," *IEEE Trans. Signal Process.*, vol. 64, no. 7, pp. 1638–1653, Apr. 2016.

[35] K. GranstrÃ¶m and U. Orguner, "A PHD filter for tracking multiple extended targets using random matrices," *IEEE Trans. Signal Process.*, vol. 60, no. 11, pp. 5657–5671, Nov. 2012.

[36] A.-A. Saucan, M. J. Coates, and M. Rabbat, "A multisensor multi-Bernoulli filter," *IEEE Trans. Signal Process.*, vol. 65, no. 20, pp. 5495–5509, Oct. 2017.

Thomas Kropfreiter Thomas Kropfreiter received the B.Sc. degree in electrical engineering and the Dipl.-Ing degree (M.Sc. equivalent) in telecommunication engineering with distinction from TU Wien, Vienna, Austria, in 2012 and 2014, respectively. He is currently working toward the Ph.D. degree in the Signal Processing Group, TU Wien. He was a visiting researcher with the Scripps Institution of Oceanography, University of California San Diego, La Jolla, CA, USA in 2021. He received the First Runner-Up Award in the student paper category at FUSION 2020. His research interests include multi-object tracking, distributed signal processing in wireless sensor networks, message passing algorithms, and finite set statistics.

Florian Meyer (S'12–M'15) received the Dipl.-Ing. (M.Sc.) and Ph.D. degrees (with highest honors) in electrical engineering from TU Wien, Vienna, Austria in 2011 and 2015, respectively. He is an Assistant Professor with the University of California San Diego, La Jolla, CA, jointly between the Scripps Institution of Oceanography and the Electrical and Computer Engineering Department. From 2017 to 2019 he was a Postdoctoral Fellow and Associate with Laboratory for Information & Decision Systems at Massachusetts Institute of Technology, Cambridge, MA, and from 2016 to 2017 he was a Research Scientist with NATO Centre for Maritime Research and Experimentation, La Spezia, Italy.

Prof. Meyer is the recipient of the 2021 ISIF Young Investigator Award and a 2022 NSF CAREER Award. He is an Associate Editor with the IEEE Transactions on Aerospace and Electronic Systems and the ISIF Journal of Advances in Information Fusion and was a keynote speaker at the IEEE Aerospace Conference in 2020. His research interests include statistical signal processing, high-dimensional and nonlinear estimation, inference on graphs, machine perception, RF-SLAM, and graph neural networks.

Franz Hlawatsch (Fellow, IEEE) received the Diplom-Ingenieur, Dr. techn., and Univ.-Dozent (habilitation) degrees in electrical engineering/ signal processing from TU Wien, Vienna, Austria, in 1983, 1988, and 1996, respectively. Since 1983, he has been with the Institute of Telecommunications, TU Wien, where he is currently an Associate Professor. During 1991-1992, as a recipient of an Erwin Schrödinger Fellowship, he spent a sabbatical year with the Department of Electrical Engineering, University of Rhode Island, Kingston, RI, USA. In 1999, 2000, and 2001, he held one-month Visiting Professor positions with INP/ENSEEIHT, Toulouse, France and IRCCyN, Nantes, France. He (co)authored a book, three review papers that appeared in the IEEE Signal Processing Magazine, about 250 refereed scientific papers and book chapters, and three patents. He coedited three books. His research interests include statistical signal processing methods and their application to inference and learning problems.

Dr. Hlawatsch was a member of the IEEE SPCOM Technical Committee from 2004 to 2009. He was a Technical Program Co-Chair of EUSIPCO 2004 and served on the technical committees of numerous IEEE conferences. He was an Associate Editor for the IEEE Transactions on Signal Processing from 2003 to 2007, for the IEEE Transactions on Information Theory from 2008 to 2011, and for the IEEE Transactions on Signal and Information Processing over Networks from 2014 to 2017. He coauthored papers that won an IEEE Signal Processing Society Young Author Best Paper Award and Student Paper Awards at IEEE ICASSP 2011 and FUSION 2020. He is a EURASIP Fellow.